Text and references accompanying Nevada Bureau of Mines and Geology Open File 15-2

# Preliminary geologic map of Cenozoic units of the central Robinson Mountain volcanic field and northwestern Huntington Valley, Elko County, Nevada

*by*

Jens-Erik Lund Snee and Elizabeth L. Miller

Department of Geological Sciences, Stanford University

2015

*Disclaimer: NBMG open-file reports are preliminary. They have not been thoroughly edited or peer reviewed.*

## INTRODUCTION

The mapped area is located in the northwestern part of Huntington Valley and the eastern Piñon Range, northeast Nevada (Figure 1). This area includes volcanic, subvolcanic, sedimentary, and metasedimentary rocks ranging in age from Mississippian to Quaternary. The geologic setting is immediately east of the east-vergent Antler thrust front and contains Paleozoic deposits of the Antler foreland basin (Diamond Peak and Chainman Formations) and the overlying Antler overlap sequence (Moleen Formation and undifferentiated limestone of Pennsylvanian–Permian age) (Smith and Ketner, 1975, 1978; Colgan and Henry, 2009).

Paleozoic units have previously been described by Smith and Ketner (1975), Stewart (1980), and Coats (1987), and include quartzite and chert conglomerates of the Mississippian–Pennsylvanian Diamond Peak Formation; silty, cliff-forming, cherty limestones of the Pennsylvanian Moleen Formation; shale and sandstone of the Mississippian Chainman Shale; and undivided platy siltstones and sandstones of Pennsylvanian–Permian age.

Although pre-Cenozoic rocks record important geologic history, particularly of Paleozoic–Mesozoic contraction that took place during the Antler and Sevier orogenies (e.g. Ketner and Smith, 1963; Smith and Ketner, 1975; Trexler and Nitchman, 1990; Ketner, 1998; Trexler et al., 2004; Dickinson, 2006), detailed mapping of these units was not the focus of the present research. This geologic map focuses on Cenozoic units for their ability to reveal important information about Cenozoic extensional tectonics near the Ruby Mountains–East Humboldt Range (RMEH) metamorphic core complex (Figure 1).

The following section describes Cenozoic units within the map area (Figure 1). The results of geochronologic and geochemical analyses conducted on these rocks are used here to establish unit ages, relationships, and names, but detailed analytical methods, results, and implications are discussed in Lund Snee (2013) and Lund Snee et al. (submitted). The geologic map is based on field mapping conducted during the summers of 2010, 2011, and 2012.

## UNIT DESCRIPTIONS

The mapped area (Figure 1) includes an impressively complete succession of Late Cretaceous(?) to Quaternary sedimentary, volcanic, and subvolcanic rocks (Figure 2). Geologic unit descriptions are drawn from Lund Snee (2013) and are also summarized in Lund Snee et al. (submitted). The results of geochronologic and geochemical analyses conducted on these units are mentioned when they help constrain stratigraphic relationships, but are discussed in detail in Lund Snee (2013) and Lund Snee et al. (submitted). Referenced sample localities are indicated on the map. Where possible, unit names and map symbols have been preserved from Smith and Ketner (1978), but modifications have been made to simplify interpretations and accommodate more recent data.

### Late Cretaceous(?)–Eocene(?) conglomerate, sandstone, siltstone, and limestone (TKcs)

Conglomerate, sandstone, siltstone, and limestone make up the lowest Cenozoic deposits above the unconformity with Paleozoic rocks, where they are often exposed as "redbeds." Smith and Ketner (1976) differentiated "limestone

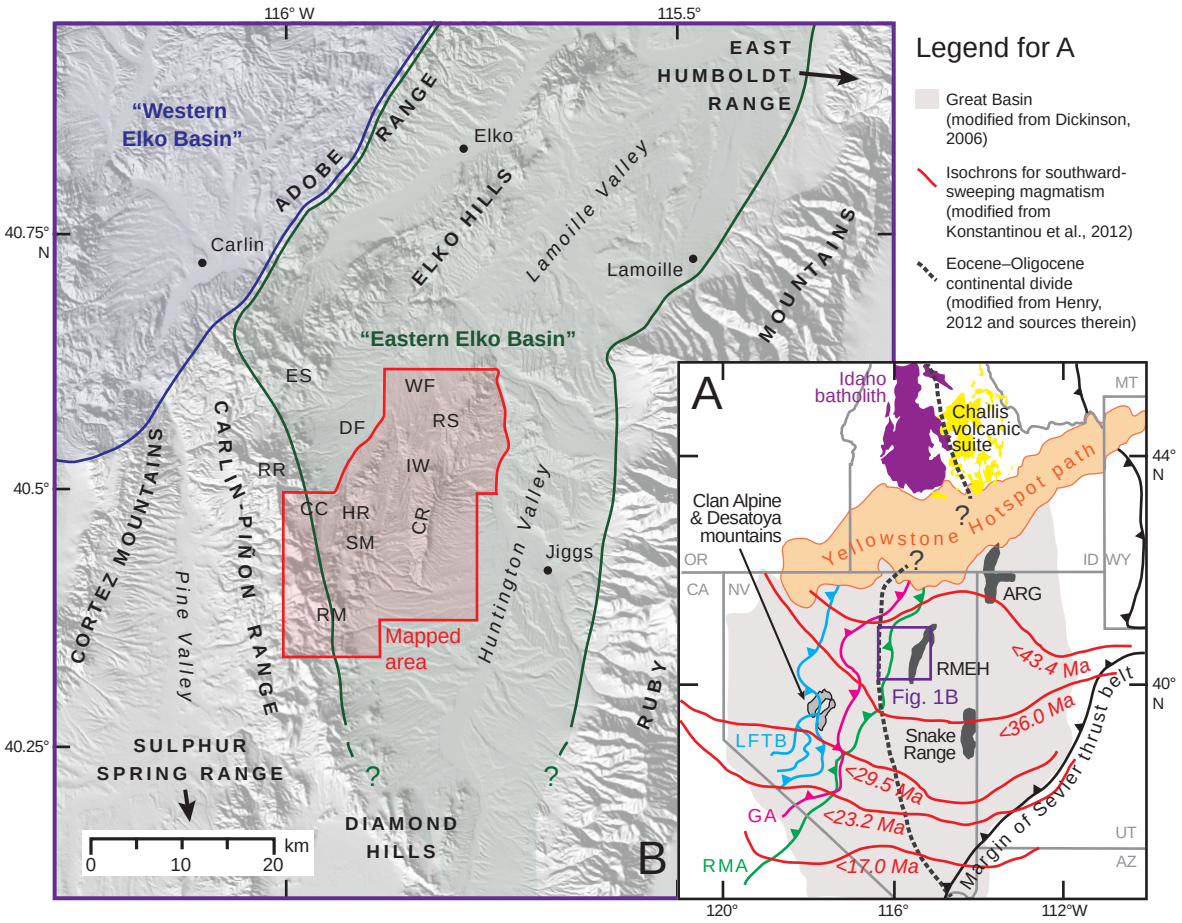


Figure 1: (A) Physiographic provinces and areas affected by important events in Cordilleran geologic history, projected on a map of present-day western North America. Map generated in GeoMapApp v.3.3.9 (Haxby et al., 2010) using the GMRT base map (Ryan et al., 2009). RMEH—Ruby Mountains–East Humboldt Range (RMEH) metamorphic core complex, ARG—Albion–Raft River–Grouse Creek Range metamorphic core complex; LFTB—Luning-Fencemaker thrust belt; GA—Golchonda allochthon; RMA—Roberts Mountains allochthon. Great Basin boundaries and Eastern margins of Golchonda and Roberts Mountains allochthons modified from Dickinson (2006). Luning-Fencemaker thrust belt location modified from Best et al. (2009). Sevier thrust front location after DeCelles (2004). Eocene–Oligocene paleodivide modified from Henry et al. (2012). Extent of Idaho Batholith and Challis volcanic field modified from Chetel et al. (2011). (B) Map of study area and surrounding region. ES—Emigrant Spring; WF—White Flats; DF—Dixie Flats; RS—Red Spring; RR—Railroad mining district; CC—Cissillini Canyon; HR—Hackwood Ranch; CR—Cedar Ridge; SM—Squaw Mountain; RM—Robinson Mountain. Eocene Elko Basin boundaries modified from Haynes (2003).

and limestone-clast conglomerate (Tcl)" from "conglomerate, sandstone, siltstone, and limestone (Tcs)." Noting greater angularity of cobbles in conglomerates and lower amounts of silt relative to limestone in their unit Tcl, Smith and Ketner (1976) proposed that clasts in this limestone unit were transported shorter distances than those in the conglomeratic sandstone and siltstone unit (their Tcs). However, the two units are likely contemporaneous, at least in part (Smith and Ketner, 1976). Outcrops of conglomerate are grayer in color and clasts are more limestone-rich nearer exposures of similar rocks in the underlying Paleozoic sequence, suggesting that Paleozoic source units are a major contributor to the different appearances of this unit in outcrop.

For these reasons, it is proposed that Tcl and Tcs of Smith and Ketner (1976) are simply different facies of the same unit, and that differentiating them is counterproductive for stratigraphic purposes. These units are now combined into unit TKcs, which refers to conglomerate, sandstone, siltstone, and limestone at the base of the Cenozoic section, and includes the grey limestone clast conglomerates.

Smith and Ketner (1976) determined a maximum thickness of 760 m for their Tcs, and 195 m thickness for their Tcl based on map measurements, due to the lack of continuous coverage of these units. We estimate a total thickness for this new combined unit (TKcs) of about 580 m (Figure 2), based also on map measurement, which is thinner than previous estimates. This could be accounted for by differing coverage of bedding readings between the two studies. The best exposures of this unit area in the map area are east of Red Spring (e.g. 40.581646°N, 115.764059°W, WGS84; Figure 1B). Bed dip is variable, ranging from gentle (~20°) to steep (>60°), and it is gently folded and faulted in places.

TKcs is clearly older than the Elko Formation, based on its stratigraphic position below the Elko Formation and the presence of dated Cenozoic volcanic material in the Elko Formation that are not detected in TKcs. This basal unit TKcs may be correlated with other basal Cenozoic clastic units in the region, such as the Sheep Pass Formation (Fouch et al., 1979; Moore et al., 1983; Ketner and Alpha, 1992; Druschke et al., 2009, 2011). Smith and Ketner (1976) found no contemporaneous volcanic material in these deposits, and detrital zircon analyses (Lund Snee, 2013) likewise detect no Tertiary age zircons in this unit. Speculative age constraints based on snail and clam fossils in TKcs are reported to be of Cretaceous to early Tertiary age (Smith and Ketner, 1976).

In some places, this unit can be readily identified by red boulder outcrops or exposures of strongly red or orange soil, but it also forms brown, tan, and grey outcrops, predominantly of limestone clast conglomerate or platy siltstone, which weather to tan and brown soil (Figures 3A and 3B). Conglomerates often form resistant, bedded outcrops that range from clast- to matrix-supported, with a rust-red–orange matrix of sand and silt (Figure 3A). The exteriors of many clasts are weathered rust-red. Clasts range in size from pebbles to cobbles, are derived from local Paleozoic rocks, and include siltstone, quartzite, chert, and limestone. Degree of rounding varies within beds from rounded to angular, suggesting varied transport distances. Elongate clasts are often aligned and plunge shallowly to the south or southeast.

Outcrop-scale fining upward sequences are observed in conglomerates, with upper layers composed of centimeter- to millimeter-scale laminations of small pebble to coarse sand clasts in a silt- to coarse sand-sized matrix. Lenses of sandstone and siltstone, with average grain sizes ranging from silt to coarse sand, are interlayered with conglomerates.

Siltstone and sandstone facies are less resistant than conglomerates and are typically exposed as platy, angular chips of tan-, orange-, or brown-weathering float (Figure 3B). Fine sandstones and siltstones are more commonly observed at upper stratigraphic levels in this unit, suggesting rapid erosion of local slopes and transition from alluvial fan (conglomerates) to shallow lacustrine (siltstone) settings. A thick succession of TKcs siltstone is exposed east of Red Spring, where platy, finely laminated beds dip up to ~70°E (Figure 1B).

In a thin section of pebbly sandstone (sample ELM11-PN16), limestone and minor clay and mud comprise the matrix between rounded to angular (mostly subrounded) sand grains (Figure 3C), and calcite partly fills rare pore spaces. Rust-red staining mantles grain boundaries and forms patches within the calcareous matrix. Volcanic rock clasts are notably absent.

## Late Cretaceous(?)–Eocene(?) limestone (TKl)

Lower Tertiary limestone (TKl) is exposed east of Red Spring, where it is generally tan, brownish purple, or elephant grey and contains chert nodules. Smith and Ketner (1976) and Smith and Ketner (1978) previously applied a symbol of Tcl to this unit. We assume that this unit was deposited during Late Cretaceous(?)–Eocene(?) time because it lacks Cenozoic volcanic detritus and appears to overlie basal Cenozoic redbeds (TKcs) thought to have a similar depositional age.

We thus apply the "limestone" (TKl) name to any limestone of Late Cretaceous or early Cenozoic age that lies stratigraphically below the Elko Formation. We estimate a total thickness for this unit of ~600 m, but true thickness is difficult to accurately measure because this unit is folded and yields generally inconsistent bedding measurements.

A dark brown–purple-weathering limestone with small (<1 cm long), dark streaks of chert (sample 12JLS170) was collected immediately above the contact with underlying conglomerate–siltstone "redbeds" (TKcs). In thin section, a micritic calcite matrix comprises the majority of the rock (Figure 4A) and narrow pore spaces up to 1 cm long fill the rest of the sample. Approximately 60% of pore space has been filled with sparry calcite (Figures 4A–B). Bioclasts including

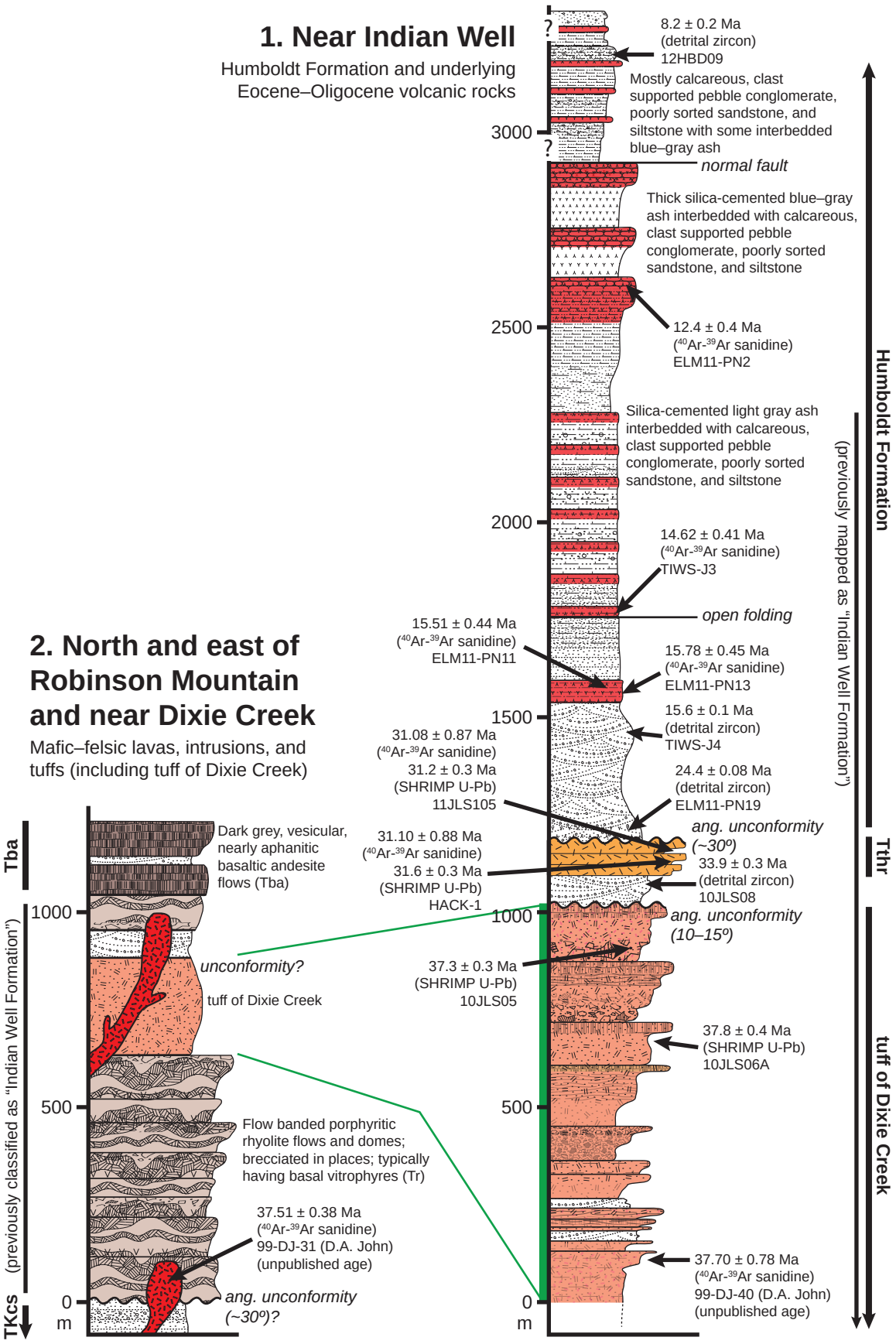
1. Near Indian Well
Humboldt Formation and underlying Eocene–Oligocene volcanic rocks
8.2 ± 0.2 Ma (detrital zircon) 12HBD09
Mostly calcareous, clast supported pebble conglomerate, poorly sorted sandstone, and siltstone with some interbedded blue–gray ash
normal fault
Thick silica-cemented blue–gray ash interbedded with calcareous, clast supported pebble conglomerate, poorly sorted sandstone, and siltstone
12.4 ± 0.4 Ma (40Ar-39Ar sanidine) ELM11-PN2
Silica-cemented light gray ash interbedded with calcareous, clast supported pebble conglomerate, poorly sorted sandstone, and siltstone
14.62 ± 0.41 Ma (40Ar-39Ar sanidine) TIWS-J3
open folding
15.51 ± 0.44 Ma (40Ar-39Ar sanidine) ELM11-PN11
15.78 ± 0.45 Ma (40Ar-39Ar sanidine) ELM11-PN13
15.6 ± 0.1 Ma (detrital zircon) TIWS-J4
31.08 ± 0.87 Ma (40Ar-39Ar sanidine)
31.2 ± 0.3 Ma (SHRIMP U-Pb) 11JLS105
24.4 ± 0.08 Ma (detrital zircon) ELM11-PN19
ang. unconformity (~30º)
31.10 ± 0.88 Ma (40Ar-39Ar sanidine)
31.6 ± 0.3 Ma (SHRIMP U-Pb) HACK-1
33.9 ± 0.3 Ma (detrital zircon) 10JLS08
ang. unconformity (10–15º)
37.3 ± 0.3 Ma (SHRIMP U-Pb) 10JLS05
37.8 ± 0.4 Ma (SHRIMP U-Pb) 10JLS06A
37.70 ± 0.78 Ma (40Ar-39Ar sanidine) 99-DJ-40 (D.A. John) (unpublished age)
3000
2500
2000
1500
1000
500
0 m
Humboldt Formation
(previously mapped as "Indian Well Formation")
Tthr
tuff of Dixie Creek
2. North and east of Robinson Mountain and near Dixie Creek
Mafic–felsic lavas, intrusions, and tuffs (including tuff of Dixie Creek)
Tba
Dark grey, vesicular, nearly aphanitic basaltic andesite flows (Tba)
unconformity?
tuff of Dixie Creek
Flow banded porphyritic rhyolite flows and domes; brecciated in places; typically having basal vitrophyres (Tr)
37.51 ± 0.38 Ma (40Ar-39Ar sanidine) 99-DJ-31 (D.A. John) (unpublished age)
ang. unconformity (~30º)?
1000
500
0 m
TKcs (previously classified as "Indian Well Formation")

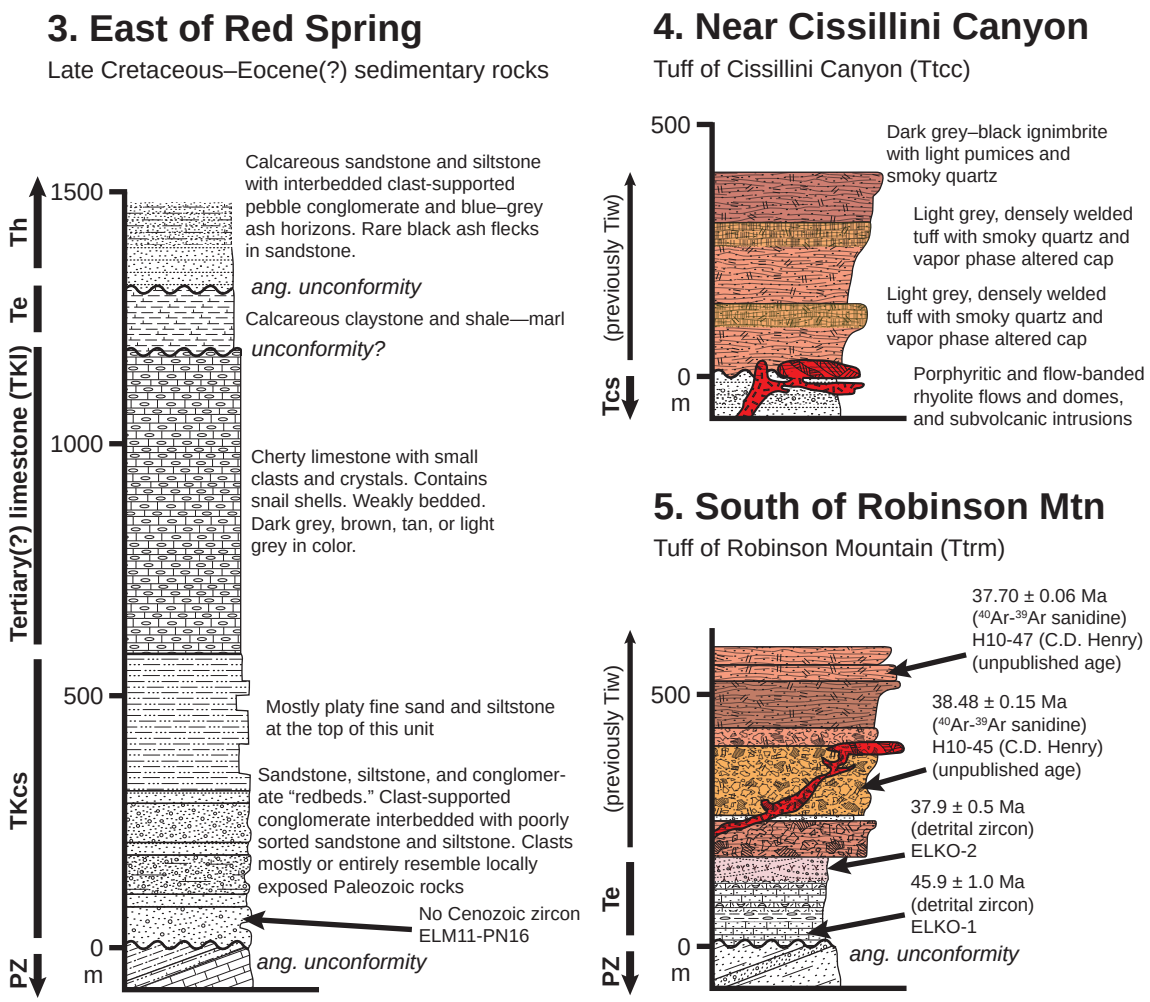


Figure 2: Stratigraphy in the mapped area (Figure 1). Section locations correspond to landmarks shown on the map. Many thicknesses were measured from the map and are hence approximate. Abbreviations: Th—Humboldt Formation; Tthr—tuff of Hackwood Ranch; Tiw—"Indian Well Formation"; Te—Elko Formation; TKcs—Late Cretaceous(?)—Eocene(?) conglomerate, sandstone, siltstone, and limestone; PZ—Paleozoic strata. See Lund Snee (2013) for geochronologic results.

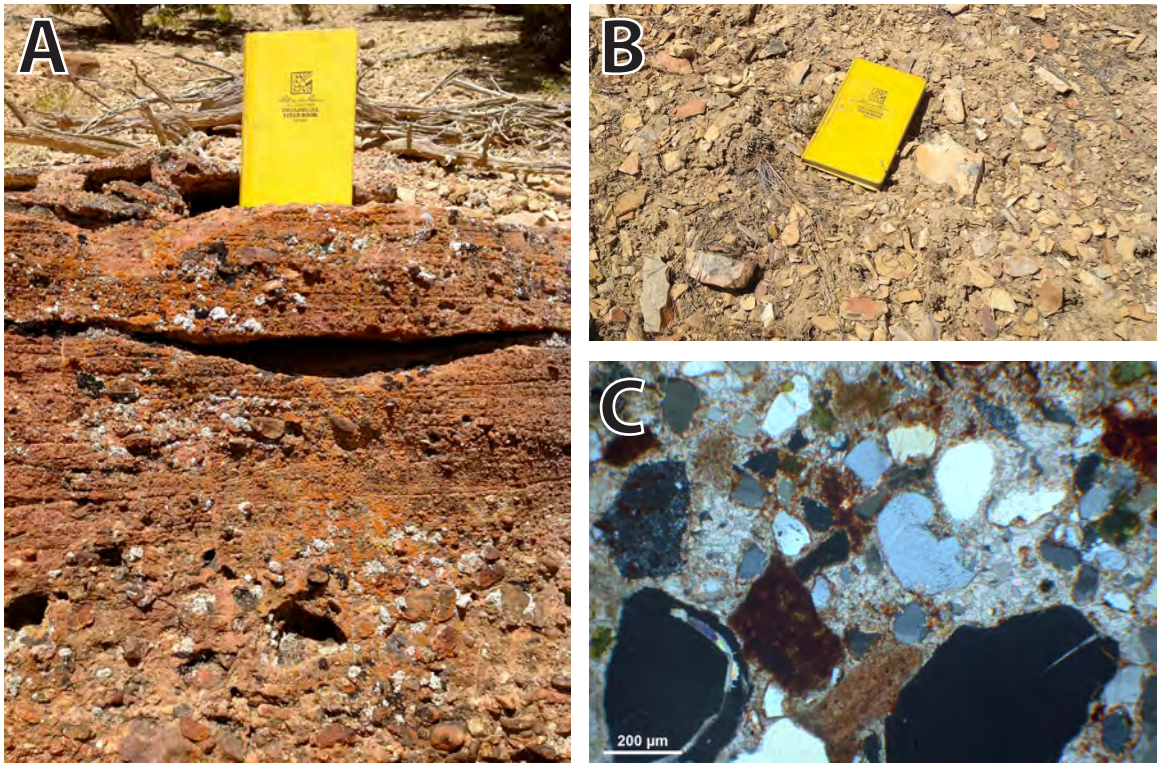


Figure 3: Late Cretaceous–Eocene(?) "redbeds" (TKcs). (A) Resistant outcrop of cemented pebble conglomerate and pebbly sandstone, with characteristic red-orange color. (B) Tan and red-orange chips of siltstone float characteristic of siltstone weathered from upper levels of this unit. (C) Photomicrograph showing clasts of quartz, feldspars, limestone, and metasedimentary rocks in a matrix of sparry calcite and mud (sample ELM11-PN16), XPL.

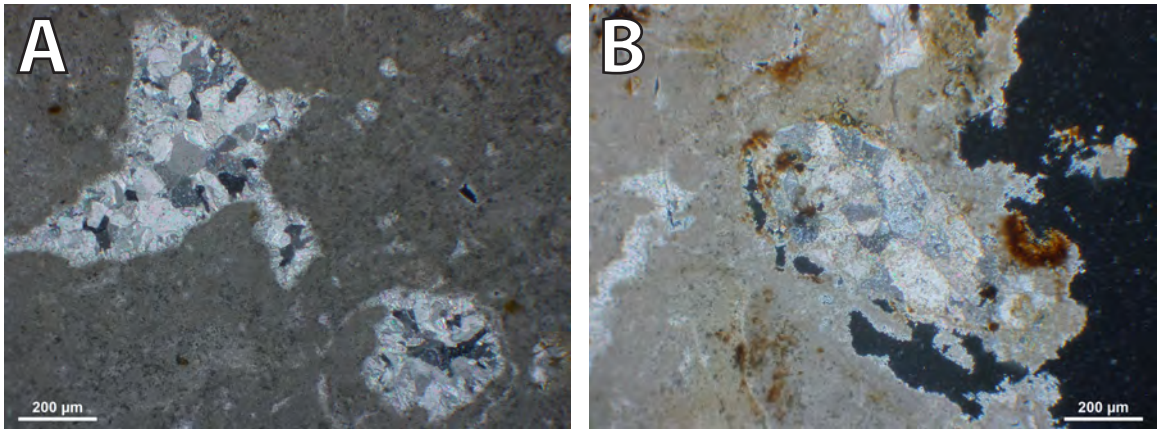


Figure 4: Photomicrographs of Late Cretaceous(?)–Eocene(?) limestone (TKl). (A) Sparry calcite filling pore space within micritic limestone matrix (sample 12JLS170), XPL. (B) Snail fossil in a matrix of micritic limestone. Open pore space occupies the eastern edge of the photograph. Sparry calcite fills pores at the west and north (sample 12JLS170), XPL.

small snail fossils are visible in thin section (Figure 4B).

## Eocene Elko Formation (Te)

The Elko Formation is a roughly fining-upward succession of boulder to pebble conglomerate, sandstone, siltstone, limestone (often with chert nodules), paper shale, and claystone deposited in a fluvial-lacustrine environment (including stream channel, floodplain, deltaic, mudflat, and lacustrine settings), and it contains tuffaceous horizons (Smith and Ketner, 1976; Solomon et al., 1979; Moore et al., 1983; Server and Solomon, 1983; Ketner, 1990; Ketner and Alpha, 1992; Haynes, 2003; Cline et al., 2005; Henrici and Haynes, 2006). Rocks of the Elko Formation in the map area were originally assigned to the Eocene Green River group of Hague and Emmons (1877) and King (1878).

Regionally, the Elko Formation is divided into a lower member (coarse clastics including boulder conglomerate and sandstone with horizons of silty shale and tuff), middle member (cherty limestone), and upper member (lacustrine siltstone, shale, claystone, and tuff) (Solomon et al., 1979; Server and Solomon, 1983; Ketner and Alpha, 1992; Haynes, 2003). Ostracode and gastropod fossils are abundant in lacustrine limestones (Solomon et al., 1979).

Haynes (2003) differentiated deposits of the eastern and western portions of the Eocene Elko Basin (Figure 1B), which are characterized by different facies. The study area is within the eastern Elko Basin, which experienced sedimentation from ~46.1–38.9 Ma and predominantly contains deposits having a lacustrine origin (Haynes, 2003; Henrici and Haynes, 2006). The Elko Basin may have been fault-bound, and paleoflow directions in the basal conglomerates are predominantly to the west and northwest (Haynes, 2003).

In the study area, the Elko Formation is characterized by laminated shale, siltstone, limestone, and claystone that are light tan, light yellow, light grey, or black (Smith and Ketner, 1976; Haynes, 2003). The Elko Formation rests on Late Cretaceous(?)–Eocene(?) conglomerate, sandstone, siltstone, and limestone (TKcs) and limestones (TKl) but also unconformably overlies Paleozoic rocks elsewhere (stratigraphic sections 3 and 5 of Figure 2).

In the study area, this unit is ~180 m thick (section 5 of Figure 2) and the lower portion contains a roughly upward-fining sequence of calcareous pebble conglomerate, sandstone, siltstone, limestone, shale, and interbedded tuff horizons, but paper shale and claystone are also interbedded within the lower coarse clastics (Figure 5). The clastic portions of the succession appear to become less calcite-rich upward. Boulder conglomerate is not exposed in the map area and pebble conglomerate is exposed only immediately above the contact with Paleozoic rocks (section 5 of Figure 2).

We dated zircons from detrital sample ELKO-1, taken immediately above the unconformable contact with Paleozoic rocks (section 5 of Figure 2). A maximum depositional age of 45.92 ± 0.48 Ma was obtained for this sample by taking the weighted mean of the youngest coherent group of ages. A second sample (ELKO-3), taken from slightly higher in the Elko Formation (section 5 of Figure 2), yielded a maximum depositional age of 45.00 ± 0.95 Ma. A third sample (ELKO-2), taken from near the contact with overlying Eocene tuffs (section 5 of Figure 2), yielded a maximum depositional age of 37.89 ± 0.46 Ma.

In thin section, sandstones of the lower Elko Formation are cemented by calcite and contain limestone clasts (Figure 6A), which distinguishes this unit from less carbonate-rich sediments that are interbedded within overlying Eocene volcanic rocks (section 5 of Figure 2). A sandstone sample (ELKO-1) taken from pebbly sandstone and pebble conglomerate at the base of the section (section 5 of Figure 2) also contains abundant moderately- to well-sorted and rounded clasts of quartz, quartzite, chert, potassium feldspar, siltstone, and shale, suggesting significant input from nearby exposed Paleozoic sources (Figure 6A). Small fossil fragments are also present in this sample. Consistent with outcrop observations, significantly less calcite cement is observed slightly higher in the lower clastic succession (sample ELKO-3; Figures 6B and 6C), where clasts are dominantly quartzite, chert, and siltstone.

The succession fines upward to calcareous sandstone and thinly bedded siltstone, and contains horizons of silty chert. Tuffaceous interbedded sandstones and pebble conglomerates (sample ELKO-2) are exposed immediately beneath the contact with the overlying Eocene tuff of Robinson Mountain (unit Ttrm; section 5 of Figure 2). In thin section, tuffaceous horizons are very rich in felsic to intermediate composition volcanic lithics (~80%), as well as clasts of plagioclase, potassium feldspar, quartz, and kinked biotite (Figures 6D–E). Siltstone clasts are rarely observed (~2%).

Limestone, siltstone, and claystone are also exposed east of Red Spring (section 3 of Figure 2) and immediately northeast of Cedar Ridge (Figure 1B). Because it is not certain whether these deposits are part of the Elko Formation, they have been marked as queried on the map, but they resemble the upper member of the Elko Formation described by Haynes (2003). These deposits are weakly bedded in places and finely laminated elsewhere, and are distinguished by their typically light tan to light yellow color (Smith and Ketner, 1976). Claystones often fracture in a conchoidal pattern. Northeast of Cedar Ridge (Figure 1B), finely laminated (1–3 mm scale), light-tan to yellow claystone is exposed near light tan limestone clast conglomerates (sample 12JLS228) containing dark grey, well rounded pebble-sized clasts of limestone and chert ($\leq$2 cm) in a silt–mud-sized matrix. In thin section, the limestone clast conglomerates contain rounded lithics of silty limestone, quartzite, and siltstone, as well as shell fragments and sparse angular to subangular clasts of plagioclase and quartz (Figure 6F).

The Elko Formation is overlain by volcanic rocks of the

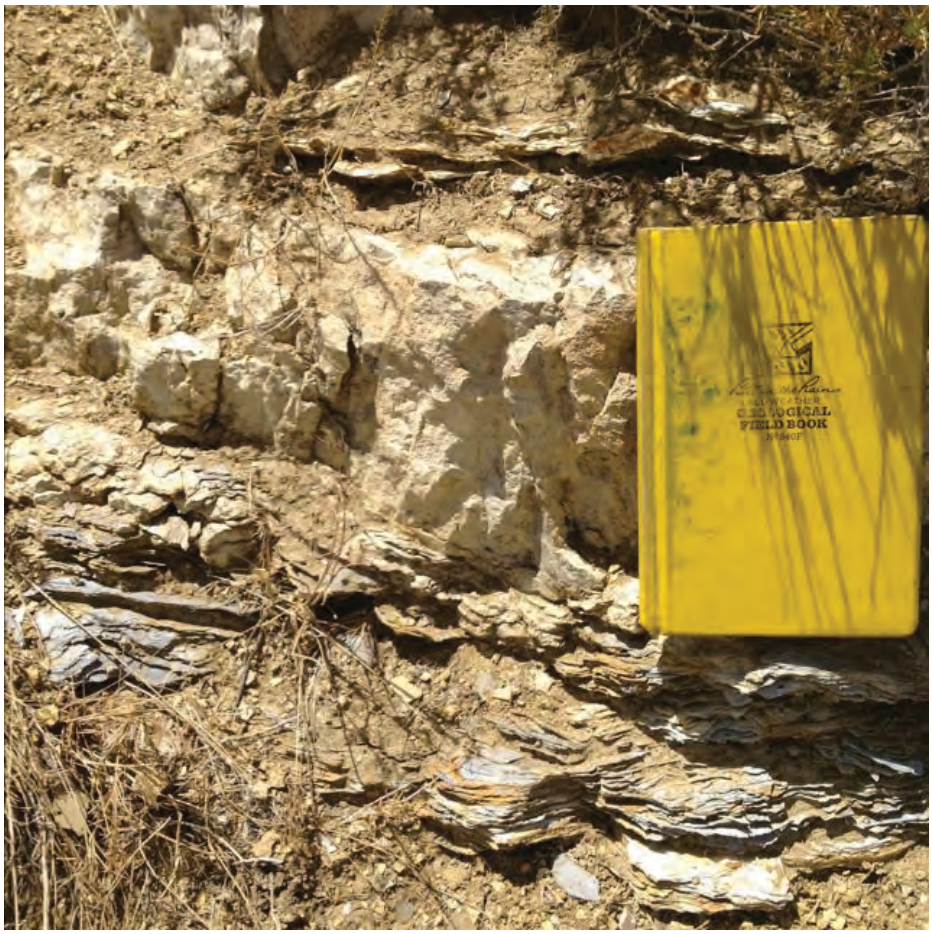


Figure 5: Photograph of Elko Formation mudstone (light tan middle and uppermost strata) and thinly laminated paper shale (blue-grey lower strata and tan upper–middle strata) south of Robinson Mountain.

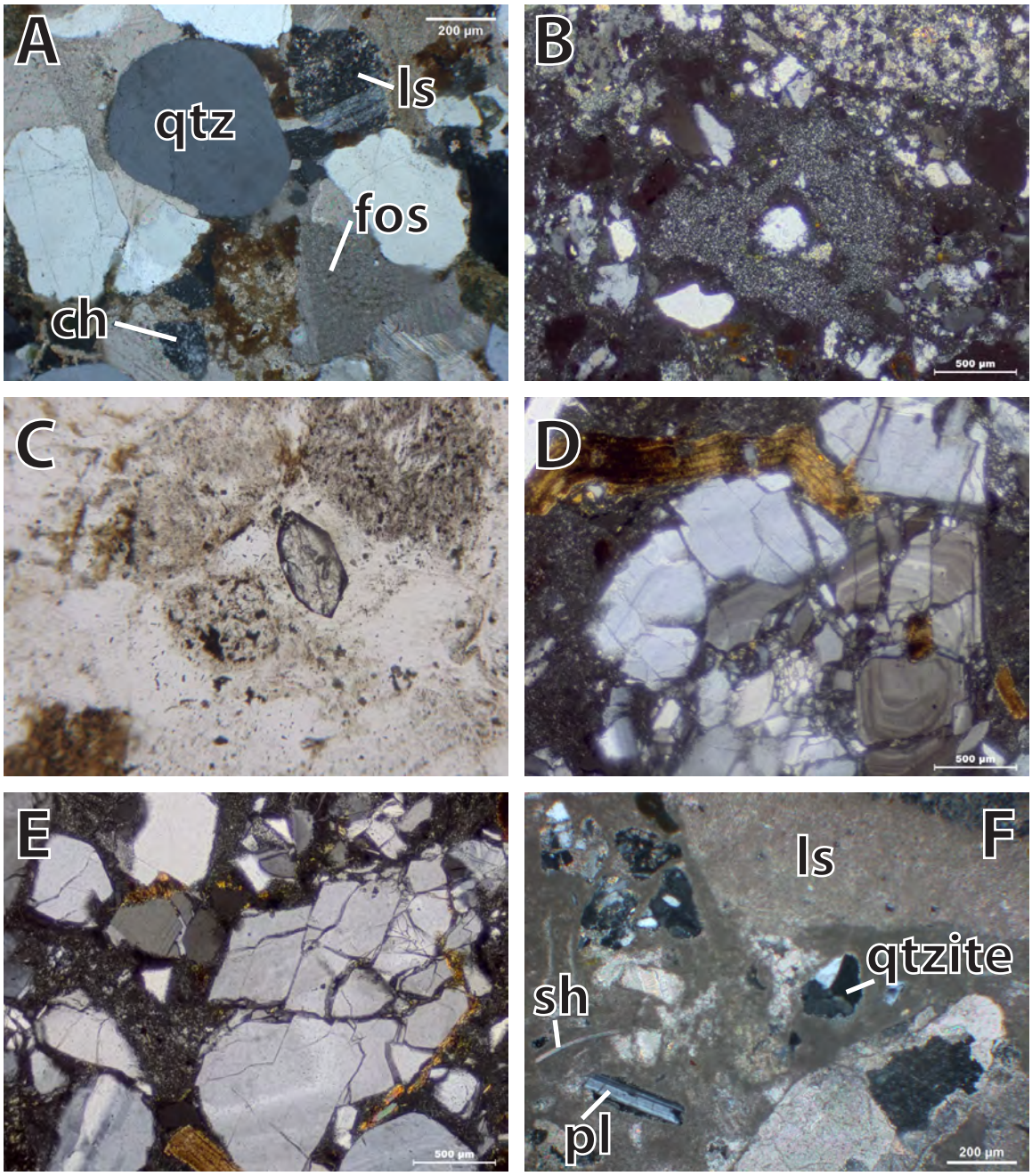


Figure 6: Photomicrographs of samples from the Elko Formation. (A) Photomicrograph of sandstone within pebble conglomerate near the base of the Elko Formation (sample ELKO-1), XPL. Rounded and subrounded quartz (qtz) and limestone (ls) grains are cemented by calcite, and angular fragments of fossils (fos) and chert (ch) are also present. (B) Photomicrograph of sandstone from a sample (ELKO-3) taken slightly above ELKO-1 but near the base of the Elko Formation (Figure 2). Siltstone, chert, and quartzite clasts are cemented mostly by silica. (C) Zircon crystal (sample ELKO-3), XPL. Field of view is ~360 µm. (D) Shattered feldspar crystals and kinked biotite in a tuffaceous horizon (sample ELKO-2) near the contact with the overlying Eocene tuff of Robinson Mountain, XPL (Figure 2). (E) Shattered plagioclase crystals in volcanic lithics in a tuff horizon (sample ELKO-2) near the contact with the overlying Eocene tuff of Robinson Mountain, XPL. (F) Limestone clast conglomerate containing shell fragments (sh), clasts of plagioclase (pl) and quartz, and lithics of limestone (ls) and quartzite (qtzite) (sample 12JLS228), XPL.

Robinson Mountain volcanic field. Some workers have proposed that the volcanic rocks are in contact with the Elko Formation across an unconformity in the study area (Smith and Ketner, 1976), but others suggest that the lower parts of thick overlying Paleogene tuffs interfinger with the upper Elko Formation in the Elko Hills (Figure 1B), where it represents the end of Eocene lacustrine deposition in the Elko Basin (Haynes, 2003).

Our mapping found no evidence for an unconformity at the contact between these units, and the similarity of dips and ages on both sides of the contact supports a conformable relationship. Andesite flows are exposed between the Elko Formation and overlying silicic volcanic rocks in places outside the map area (Server and Solomon, 1983; Haynes, 2003) but none are exposed at this stratigraphic position in the study area (section 5 of Figure 2).

## Eocene rocks of the Robinson Mountain volcanic field

Eocene and Oligocene volcanic rocks in the map area were first named the Dixie Group by Hague and Emmons (1877) and King (1878). The "Indian Well Formation" name (now discontinued) was first applied by Smith and Ketner (1976) to tuffs and tuffaceous sedimentary rocks near the Piñon Range that were originally thought to be Oligocene in age, after a water well of that name in what is now mapped as latest Oligocene–Miocene Humboldt Formation (this study).

Smith and Ketner (1978) divided the "Indian Well Formation" into members containing primarily tuffs ("Tiwt"), >1000 m tuffaceous sedimentary rocks ("Tiws"), and basal tuffs and tuffaceous sedimentary rocks ("Tiwb"). The "Indian Well Formation" name was abandoned by Lund Snee (2013) because of the discovery that nearly all sedimentary rocks originally assigned to it are actually Miocene in age. They have accordingly been re-assigned to the Miocene Humboldt Formation.

The Eocene rocks of the Robinson Mountain volcanic field were previously included within the Indian Well Formation but we instead subdivide them in this section on the basis of age, composition, and map extent. Minor Paleogene age tuffaceous sediments have been classified as undifferentiated Eocene–Oligocene sedimentary rocks (Ts).

### Tuff of Cissilini Canyon and associated subvolcanic and sedimentary rocks (Ttcc)

The tuff of Cissilini Canyon is exposed at the northwest corner of the field area (Figure 1B) and further north. Based on field relations, including apparent contact with underlying Late Cretaceous(?)–Eocene(?) redbeds (TKcs), these crystal vitric ignimbrites and rhyolite flows and domes (transitional to subvolcanic intrusive rocks) are likely among the oldest rocks in the Robinson Mountain volcanic field and may be coeval with the tuff of Robinson Mountain. The Cissilini Canyon deposits are at least 400 m thick.

In the mapped area, these volcanic units form mostly isolated exposures but are more voluminous to the north. There are no ages for these rocks in the field area. Sanidines from a biotite quartz-feldspar intrusion on Bunker Hill, outside of the mapped area to the northwest, yielded a sanidine $^{40}Ar/^{39}Ar$ age of 37.38 ± 0.16 Ma (Ressel and Henry, 2006).

**Rhyolite lavas and transitional subvolcanic intrusive rocks** Flow-banded rhyolite flows and domes exposed near the tuff of Cissilini Canyon are dark to medium grey on a fresh surface but weather red-brown. The flows are moderately crystal rich, with felsic phenocrysts up to 4 mm set in a dark, glassy matrix. Rhyolite flows are often brecciated, containing clasts of identical flow-banded rhyolite, as well as some entrained clasts of tuff.

Flow-banded, crystal-rich rhyolite domes, transitional with subvolcanic intrusions, are exposed as prominent, isolated hills. Color, texture, and phenocryst composition vary between two similar endmembers: (1) very feldspar-rich (~30% of total rock), medium "elephant" grey, biotite-rich, and strongly flow-banded; (2) vaguely flow-banded and medium-grey with tan–yellow–green tint, having abundant biotite phenocrysts up to ~5 mm and indeterminate quartz. In addition, a strikingly white, vaguely flow-banded subvolcanic intrusion (Tsviw) whose subvertical, tabular form suggests a stock or dike (sample 12JLS149), is exposed in the far northwestern corner of the Robinson Mountain quadrangle.

**Ignimbrites** The tuff of Cissilini Canyon is typiclly distinguished by smoky quartz. Most cooling units (Ttcc) are ashy, poorly to densely welded, and white, light grey, tan, or light pink in color. This tuff is rich in phenocrysts of euhedral biotite, smoky quartz ($\leq$3 mm), and feldspars ($\leq$2 mm but some exposures are crystal-poor), as well as light-colored pumice. These crystal vitric tuff flows resemble the tuff of Dixie Creek but generally contain smokier quartz and are occasionally more densely welded. At least two separate flows are in stratigraphic contact at the northwestern corner of the mapped area; each has a columnar jointed and vapor phase-altered cap with light green tint (section 4 of Figure 2). Similar tuff is exposed in isolated patches nearby, perhaps indicating more than two flows.

In thin section (sample 12JLS146) quartz (35% of phenocrysts), biotite (15%), and plagioclase (40%) phenocrysts are resorbed, but sanidine (~10%) is generally fresh (Figure 8A). Lithics (~10%) include angular volcanic rocks and subrounded siltstone and chert. The degree of welding varies with stratigraphic level within each flow (section 4 of Figure 2) but it is typically densely welded.

A second cooling unit (sample 12JLS148) is lithic- and crystal-rich and poorly to densely welded, with a glassy, dark grey matrix that strongly contrasts with light grey, unflat-

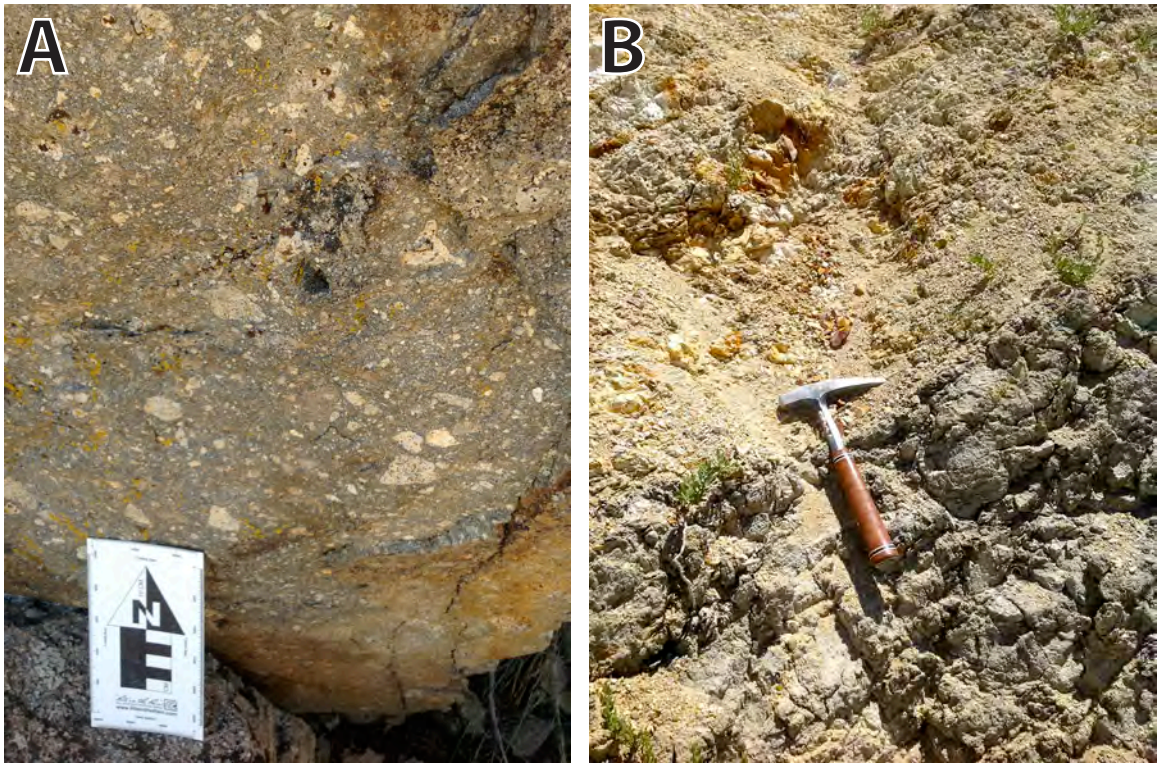


Figure 7: Photographs of the tuff of Cissilini Canyon and associated rocks. (A) Dark grey crystal lithic tuff with white pumice. (B) An angular contact between weakly bedded pumiceous sediments and overlying crumbly white and light orange silty limestones (both units mapped as Ts). This exposure southeast of Cissilini Canyon illustrates some minor degree of tilting between deposition of two thin sedimentary layers of unknown but probably Paleogene age.

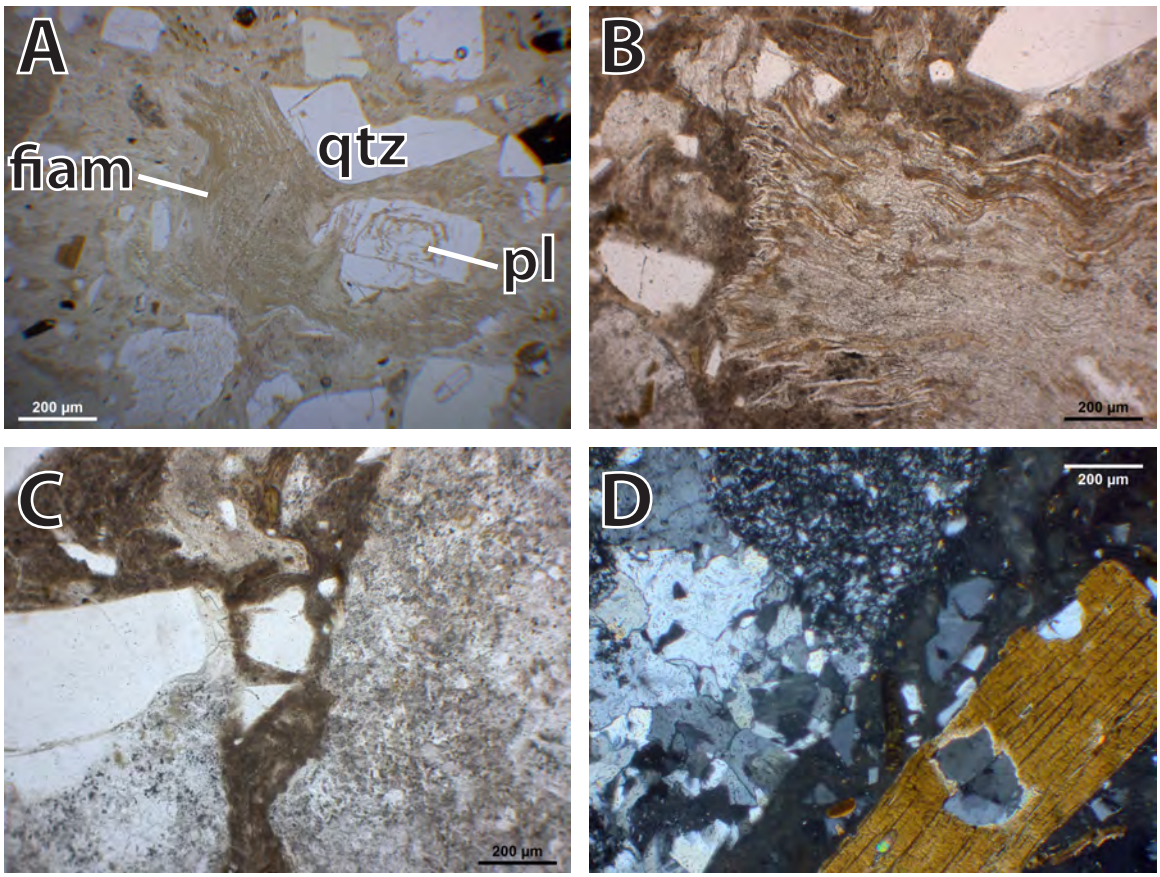


Figure 8: Photomicrographs of samples from the tuff of Cissilini Canyon. (A) Fiamme (fiam) and glassy matrix in a light-grey crystal vitric tuff (sample 12JLS146), PPL. Phenocrysts are mostly plagioclase (pl) and quartz (qtz), with minor biotite. (B) Fiamme in a dark grey crystal lithic tuff cooling unit (sample 12JLS148), PPL. (C) Lithics of porphyritic volcanic rocks in dark grey crystal lithic tuff (sample 12JLS148), PPL. Aligned brown material is glassy matrix and a small pumice is at the N edge. (D) Clasts of quartzite (SW corner) and chert (NW corner) in dark grey crystal lithic tuff (Ttcc), with a biotite crystal enclosing a zircon crystal (sample 12JLS148), XPL.

tened to fiamme-shaped pumice (section 4 of Figure 2; Figure 7B). Lithics are mostly volcanic and up to ~15 cm, and phenocrysts of smoky quartz, plagioclase, and biotite are visible in hand sample. In thin section, phenocrysts (~24%) are up to 5 mm and include quartz (55% of phenocrysts; usually with embayed margins), biotite (10%), plagioclase (30%), and sanidine (~10%). Lithics comprise ~50% (Figure 8A–D).

**Sedimentary rocks** Isolated exposures of tuffaceous sedimentary rocks are exposed in the northwest corner of the mapped area, near exposures of the tuff of Cissilini Canyon, and appear to be synchronous with or to slightly postdate the volcanic rocks. Most sediments are white to medium grey and vaguely bedded and form outcrops that are crumbly, rounded masses. The matrix is generally ashy and contains biotite, feldspars, and quartz. Quartz is often moderately smoky to light pink (rosy). White to light yellow, generally unflattened ashy pumice is common.

In one location (Figure 7B; 40.485676°N, 115.958083°W, WGS84), weakly bedded, grey pumiceous sedimentary rocks (Ts) are overlain across a gentle angular unconformity by crumbly white and light orange silty limestones with wavy laminations that contain no obvious pumice (sample 12JLS141). The overlying sediments are interpreted to represent the existence of a shallow lacustrine setting following (or during a long lull in) volcanic activity.

### Tuff of Robinson Mountain (Ttrm)

The Eocene tuff of Robinson Mountain is a heterogeneous, mostly moderately–densely welded lithic to crystal ignimbrite that is best exposed to the south of Robinson Mountain (Figures 1B and 9A). This tuff may spatially and by definition overlap in part with the "Porter Complex" of Palmer et al. (1991). This tuff is not exposed further north and appears to be in depositional contact with the overlying (and slightly younger) tuff of Dixie Creek. The lowest cooling unit is in apparently conformable contact with the underlying Elko Formation.

Sanidines from an upper flow and the lowermost flow were previously dated by $^{40}Ar/^{39}Ar$, giving ages of 37.70 ± 0.06 Ma (sample H10-47) and 38.47 ± 0.15 Ma (sample H10-45), respectively (unpublished ages by C. Henry, pers. comm., 2011). A small, flow-banded, red-brown rhyolite dome is intruded between tuff layers in one location (Figure 9A) and resembles voluminous rhyolite flows and domes exposed to the east and northeast of Robinson Mountain.

This tuff forms distinctive and predictable stratigraphy in places (section 5 of Figure 2; Figure 9A). The lowest flow is a cliff-forming, moderately welded, light grey lithic tuff that contains lithics of reddish–purple chert and quartz-bearing white felsic volcanic rocks up to 2 cm, as well as sparse biotite, quartz, and plagioclase crystals, and small pumice (section 5 of Figure 2). This flow is overlain by a rhyolitic, poorly welded, gently dipslope-forming, crystal lithic tuff that contains abundant euhedral biotite and small (≤1 mm) feldspar, as well as small (≤2 cm), sparse white pumice (section 5 of Figure 2). This flow erodes to characteristic light yellow- to rust-orange-colored rounded boulders. In thin section (sample 12-YB-01), it contains abundant pore space (~15%) and a glassy, hypocrystalline matrix (Figure 9B). Lithics (~35%) are composed of porphyritic, felsic–intermediate volcanic rocks and siltstone. Crystals (~28%) are composed of occasionally embayed quartz, sanidine, zoned plagioclase, and fine (≤1 mm) biotite.

This "yellow boulder flow" is overlain by a moderately–densely welded, weakly cliff-forming, dark grey crystal tuff (Trmd; sample 12-DK GRAY-01; section 5 of Figure 2; Figure 9A) that contains sparse lithics up to 8 cm and is rich in biotite and moderately smoky quartz. Lithics (7%) are composed of volcanic rocks and poorly sorted sedimentary rocks containing fresh quartz, biotite, plagioclase, and sanidine of apparent volcanic origin (Figure 9C). Crystals (55%) include embayed quartz (up to 5 mm), green hornblende, fresh biotite, sanidine, and plagioclase (Figure 9D). Flattened fiamme (33%) with little to no pore space are observed in thin section (Figure 9D). The remaining ~5% is glassy matrix.

This "dark grey tuff" is overlain by two densely welded, strongly cliff-forming, light grey, rhyolitic, vitric crystal tuffs that have nearly identical appearance (section 5 of Figure 2; Figure 9A). Lithics are sparse and up to 1 cm. Abundant pumice (≤10 cm) weathers in negative relief. Biotite and moderately smoky quartz (≤5 mm) are abundant. In thin section (sample 12CH01), this tuff is very crystal-rich (~42%), displays strongly eutaxitic texture, and is generally devitrified (Figure 9E). Lithics (~2%) are minimal and include siltstone and volcanic rocks. Crystals include plagioclase (~38%), occasionally embayed quartz (~30%), sanidine (~20%), slightly altered biotite (~10%), and green hornblende (~2%). The section is likely repeated to the east (southeast of Robinson Mountain, e.g. 40.382436°N, 115.911385°W, WGS84) by a down-to-the-east normal fault, where gently folded, strongly cliff-forming tuffs resembling these light grey vitric crystal tuffs are exposed. In thin section, these tuffs (sample 12JLS131; Figure 9F) have nearly identical mineralogy, devitrification, and degree of welding as the main exposure (sample 12CH01).

Map relations suggest that these cliff-forming crystal vitric tuffs are overlain by a purple-weathering, dark grey (on fresh surface) vitric crystal tuff (Figures 9A and 9G), but the contact is not directly observed. In thin section, the purple-weathering flow is very crystal-rich (~40%), contains sparse lithics (~5%) of metasedimentary rocks and devitrified rhyolitic subvolcanic intrusion or lava, and contains crystal-rich fiamme (~25%) and a devitrified matrix (~30%) (sample 12JLS220; Figure 9H). Mineralogy includes plagioclase, occasionally resorbed quartz (≤5 mm), sanidine, biotite, and minor green hornblende (Figure 9I).

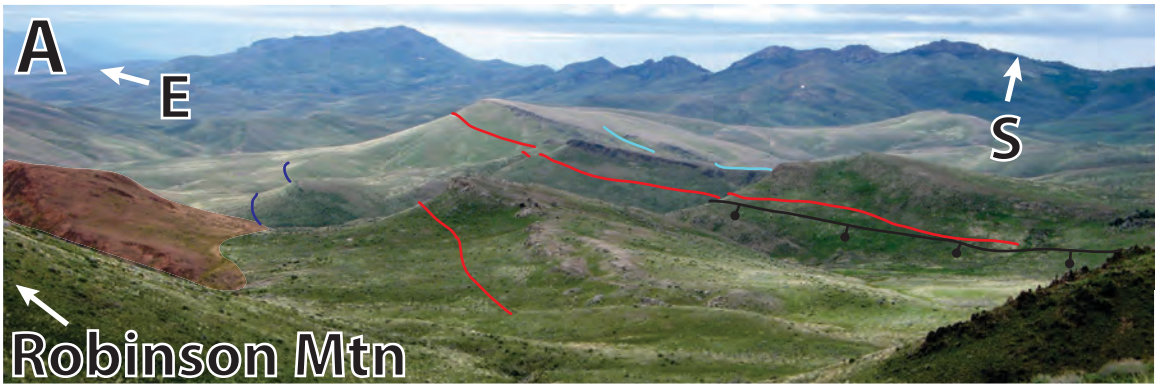
A
E
S
Robinson Mtn


B
200 µm
qtz
ves

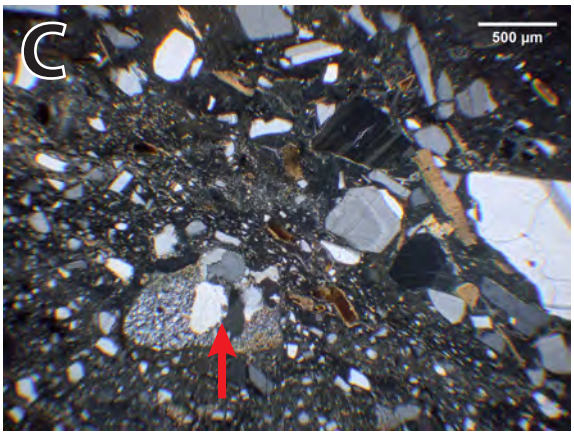
C
500 µm


D
qtz
200 µm

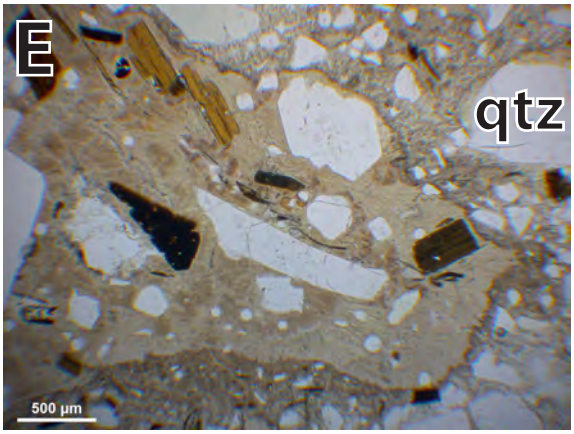
E
qtz
500 µm

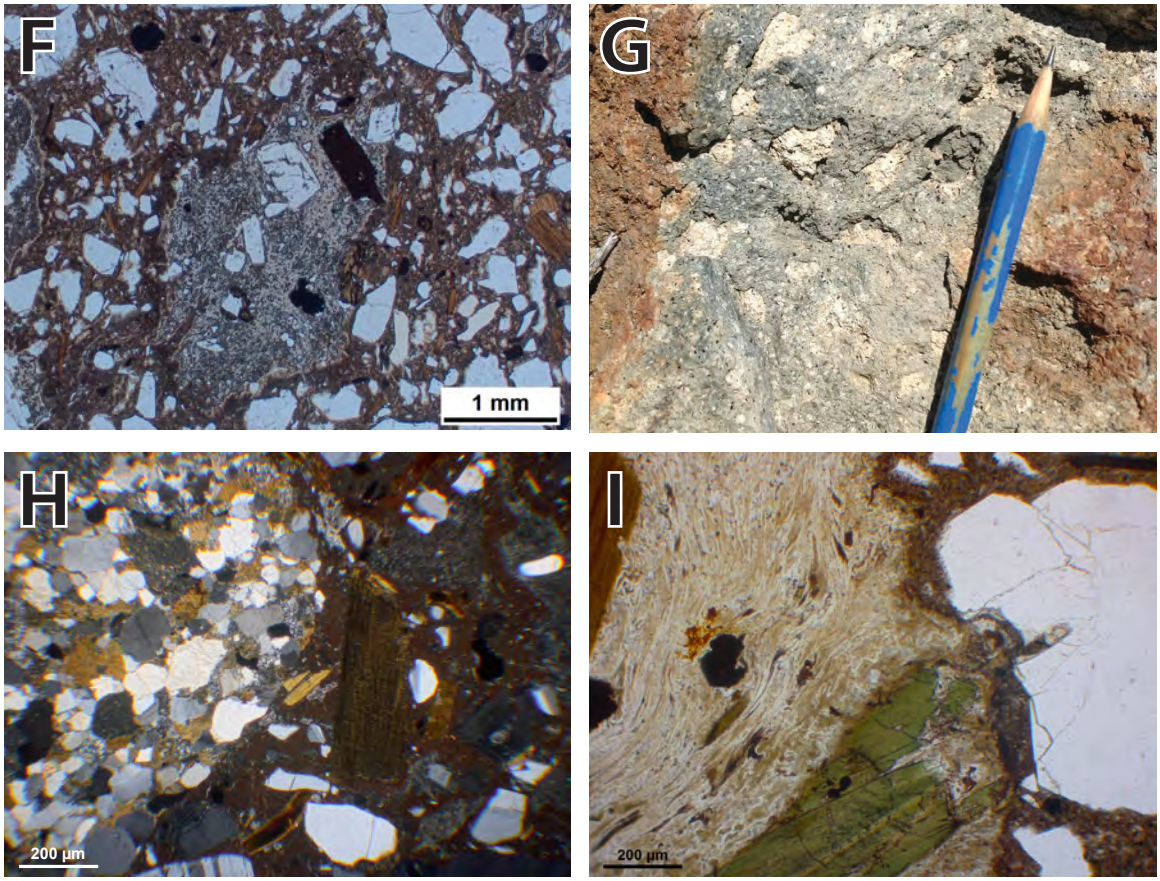


Figure 9: (A) View to the southeast from the southwest flank of Robinson Mountain. Dipslopes are the tops of cooling units within the tuff of Robinson Mountain. Light blue line is the approximate base of the upper strongly welded, cliff-forming crystal vitric tuff. Red line is the approximate base of the lower strongly welded crystal vitric tuff. Dark blue line is the approximate base of the dark grey crystal tuff. Red shading represents a small rhyolite dome intruded into the tuff of Robinson Mountain. Black line is the trace of a minor normal fault (ball on downthrown side). (B) Photomicrograph of the yellow boulder-forming crystal lithic tuff, which is the second from the bottom flow (sample 12-YB-01), XPL. Visible are a quartz crystal (qtz), two rounded volcanic clasts, minor biotite, and part of a large vesicle (ves). (C) Photomicrograph of a sedimentary lithic inside the dark grey crystal tuff (sample 12-DK GRAY-01), XPL. This sedimentary lithic contains quartz, biotite, and feldspars of apparent volcanic origin, as well as a small clast of siltstone which itself contains a clast of quartzite (arrow points toward quartzite clast). (D) Photomicrograph showing a densely welded portion of the matrix of the dark grey crystal tuff (12-DK GRAY-01), as well as green hornblende, thin biotite, quartz (NE corner; "qtz"), and plagioclase (center and W edge). (E) Photomicrograph of the upper of two strongly welded, cliff-forming crystal vitric ignimbrites near the top of the tuff of Robinson Mountain (sample 12CH01) displaying phenocrysts of quartz (NE corner; "qtz"), plagioclase (upper center), biotite, and accessory zircon (small high relief mineral in center). (F) Photomicrograph of a sample (sample 12JLS131) taken from a densely welded, cliff-forming, crystal vitric tuff that is correlated with a similar flow (E) and illustrates duplication of the section across a down-to-the-east normal fault, PPL. (G) Photograph of the purple-weathering, dark grey vitric crystal tuff (e.g. sample 12JLS220). (H) Photomicrograph of a rounded metasedimentary clast (W half of image) in the purple-weathering, dark grey vitric crystal tuff within the tuff of Robinson Mountain (sample 12JLS220), XPL. The lithic contains fused quartz crystals, grains altered to clay, and clasts of chert. The E half of the image is ignimbrite groundmass. A small volcanic clast is near the NE corner. (I) Photomicrograph of the purple-weathering, dark grey vitric crystal tuff (sample 12JLS220), PPL, showing fiamme (W part of image) containing green hornblende, opaques, and biotite phenocrysts. E part of image includes a large plagioclase crystal in a devitrified matrix.

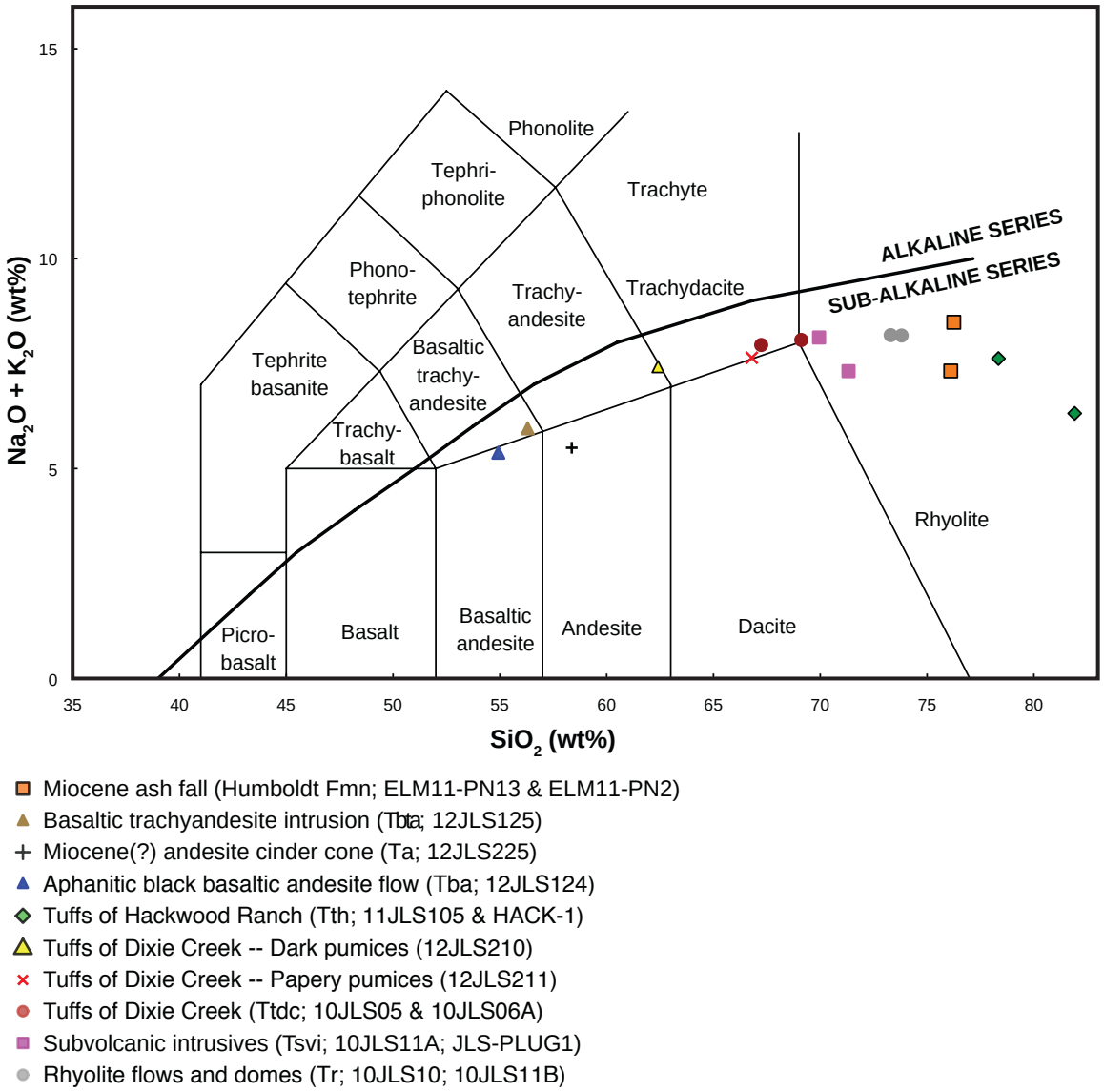


Figure 10: Total alkali versus silica (TAS) plot for the samples analyzed by Lund Snee (2013). Volcanic rock classification boundaries are from Le Bas et al. (1986). Alkaline–sub-alkaline series boundary after Rickwood (1989).

Figure 11: Stratigraphic column of ignimbrites composing the tuff of Dixie Creek.

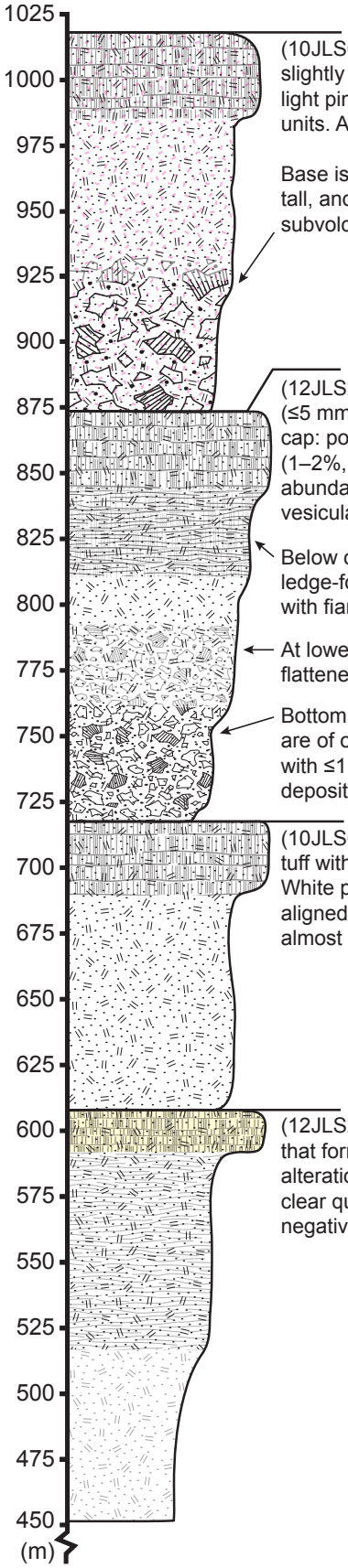


(10JLS05). White–light grey, poorly welded tuff containing biotite (≤3 mm) and slightly smoky quartz ≤7 mm. Pumices are ≤12 cm (mostly ≤1 cm) and display light pink coloration that suggests higher temperatures than many other flow units. At upper levels, pumices are flattened but retain vesicles.

Base is white, with barely flattened pumices, forms rounded boulders ~7 m tall, and is composed of ~10% angular clasts of other Tuffs of Dixie Creek and subvolcanic intrusions. Resistant cap is exposed above.

(12JLS217). Light grey tuff. Crystal-rich matrix and pumices with clear quartz (≤5 mm), hexagonal biotite (≤5 mm), and clear feldspar. Strongly cliff-forming cap: poorly welded, vapour-phase altered, and columnar jointed; sparse lithics (1–2%, ≤3 cm, volcanic); abundant crystals (25–30% of matrix and pumices); abundant (~30%), flattened, white–light grey ovoid pumices (≤6 cm, ~30%, vesicular, negative relief on eroded surfaces).

Below cap, less vapour-phase alteration; outcrop is more rounded but still ledge-forming. Lithics increase to >3% below cap and welding is moderate, with fiamme-shaped glassy pumices mostly lacking vesicles and relief.

At lower levels, color whitens, welding poorer (ashy, vesicular pumices barely flattened), and lithics 7%. Outcrop less resistant, forming rounded boulders.

Bottom of unit is very lithic-rich (≤50 cm) and mostly clast-supported. Lithics are of other Tuffs of Dixie Creek flows and rare, smaller dacite lavas or Tsvi with ≤1 cm sanidine phenocrysts. Could also be a base surge or avalanche deposit but no crossbeds nor graded pumices visible.

(10JLS06A, 10JLS06B). Strongly cliff-forming, light grey, poorly welded, ashy tuff with resistant, columnar-jointed, likely vapour-phase altered upper level. White pumices (≤10 cm; ~20%) are flattened and ovoid with moderately aligned biotite. Tuff is very quartz-rich (≤8 mm crystals), with visible biotite and almost no lithics (volcanic; <1%).

(12JLS213). Light grey, poorly–moderately welded tuff with slight yellow hue that forms prominent cliffs and dipslopes with columnar jointing: vapour-phase alteration at upper levels. Welding poor at top; increasing downward. Contains clear quartz (≤6 mm), biotite (≤2 mm), white ovoid pumices (≤15 cm; 15%) in negative relief that decrease downward, and volcanic lithics (≤3 cm; ~1%).

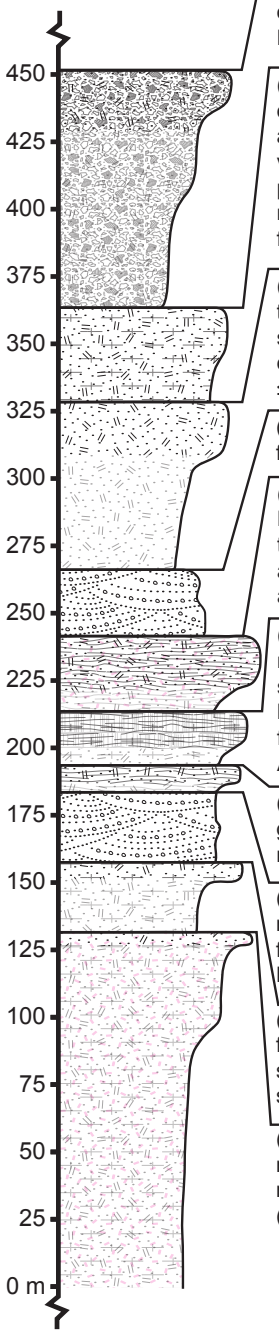


(12JLS212). Light grey, poorly welded, ledge-forming tuff with ≤12 cm (mostly ~3 cm) white–light tan moderately flattened, ovoid pumices composing ~15% of the tuff. Very biotite-rich (≤5 mm cystals), with mostly clear quartz (≤7 mm). Red, tan, and grey volcanic lithics (≤5 cm) comprise ~7% of the rock.

(12JLS209, 12JLS210, 12JLS211). Light grey tuff with moderately smoky quartz in crumbly clusters (≤1 cm), abundant biotite (≤3 mm), and mostly angular (but some rounded) volcanic lithics (≤5 cm). Pumices (<6 cm) contain vesicles visible with hand lens but slightly flattened (poor welding). Three pumice types: dominant white–light grey lumps (12JLS209); fine-grained, medium-grey, biotite-rich (12JLS210); and dull medium-grey, fine-grained with fibrous “papery” texture very rich in aligned biotite (12JLS211).

(12JLS208). Poorly welded, light grey, cliff-forming tuff with 20–25% light grey to white ashy pumices (≤9 cm) that are exposed in positive relief on eroded surfaces and grade upward to lower percentages. Tuff is biotite-rich, with clear quartz in crumbly clusters ≤7 mm and white feldspar, as well as volcanic lithics ≤4 cm that make up ~5% of the rock.

(12JLS215). Crystal-rich, poorly sorted, pumice-poor, arkosic sediments; only float observed.

(12JLS206). Light grey, red-orange-weathering moderately welded tuff. Pumices (≤15 cm): erode in negative relief; flattened (mostly 2 cm long, 5 mm thick); many glassy, with pink and dark grey glass horizons and weak biotite alignment. Moderately–smoky quartz (≤5 mm). Hexagonal biotite (<3 mm) less abundant than in lower units.

(12JLS205, 12JLS207). Light grey, moderately welded, pumice-rich (35–40%), ridge-forming tuff with clear quartz ≤4–5 mm, hexagonal biotite ≤3 mm, and sparse lithics ≤3 cm. Pumices (positive relief; ≤10 cm); most light tan & ashy, but some dull medium-grey with finer-grained papery texture. Most moderately flattened and some black, glassy, and transitional between fiamme and ovoid. Angular volcanic lithics (5–7%; ≤8 cm). Vaguely columnar jointed.

(12JLS204). Ledge-forming light-grey tuff. Pumices (≤6 cm) often glassy & dark grey, forming “fiamme” shapes (moderate welding). Lithic-poor. Clear quartz ~7 mm, biotite ≤3 mm, white feldspar ≤2 mm.

(12JLS189). Poorly sorted, cross-bedded arkosic sedimentary rocks of same mineralogy as Tuffs of Dixie Creek: quartz ≤3 mm, clear sanidine, and biotite flakes aligned parallel to bedding. Average grain size medium–coarse sand. Rosy to rust-red volcanic clasts ≤1 cm. May be a base surge deposit.

(12JLS203, 12JLS188, 12JLS206). Ashy, poorly welded, light-grey, mound-forming. Mildly smoky quartz (≤7 mm, avg. ~2 mm), hexagonal biotite (≤3 mm), sanidine, sparse volcanic lithics (≤3 cm). Pumices (≤8 cm; negative relief): some light pink; others fine-grained, medium grey, with papery texture.

(12JLS202). Light-grey poorly–moderately welded tuff with smoky quartz (≤5 mm), biotite (≤2 mm), white feldspar (≤2 mm). Forms elongate mounds with rounded boulders. Sparse volcanic lithics ≤3 cm. Light pink–light grey ovoid (partially flattened) pumices ≤3 cm (mostly <1 cm) with almost no relief.

### Eocene tuff of Dixie Creek (Ttdc) and associated rhyolite flows and domes (Tiwr)

**Ignimbrites** The tuff of Dixie Creek is a package of light gray, poorly to moderately welded crystal vitric ignimbrites (Figure 11), which appears to contain at least ~12 flow units, and is best exposed at Dixie Creek near Hackwood Ranch (e.g. 40.8232°N, 115.9122°W, WGS84; Figure 1B). Major element geochemistry of pumice identifies these ignimbrites as weakly peraluminous, calc-alkaline trachydacites (Figure 10). Previous workers have referred to this group as the "tuff of Jiggs" (Palmer et al., 1991), but its proximity to Dixie Creek, rather than the town of Jiggs, warrants the new name. The ignimbrites have a measured thickness of ~1045 m (Figure 11) but are likely thicker and may contain more flows above and below the measured section. The tuff of Dixie Creek thins southward toward Robinson Mountain. The tuff of Dixie Creek were erupted between 37.8 ± 0.4 Ma (sample 10JLS06A; Lund Snee, 2013) and 37.3 ± 0.3 Ma (sample 10JLS05; Lund Snee, 2013).

The tuff of Dixie Creek provides an excellent view of compositional and textural changes that occur during eruption of a single ignimbrite, particularly where multiple cooling units are well exposed in a canyon of Dixie Creek slightly southwest of Hackwood Ranch (Figures 1B and 11). A resistant, poorly welded, typically vapor-phase altered, and weakly columnar jointed cap often forms dipslopes at the tops of individual cooling units (Figure 12A). This cap usually overlies a moderately welded, somewhat less resistant, ashy middle layer that contains slightly more lithic material (~2–5%) than the lithic-poor cap. The lower parts of many flows, where exposed, are usually very lithic-rich and occasionally lithic-supported, with a poorly welded, ashy, pumice-poor matrix. Weathering of the tuff of Dixie Creek, particularly of areas below the resistant upper cap, forms distinctive light grey, rounded boulders, which are often weathered to be slightly overhanging.

The tuffs are quartz- and biotite-rich, with clear to moderately smoky phenocrysts ranging from 2–8 mm in diameter. In some flows, quartz crystals form crumbly clusters $\leq$1 cm diameter. There is little variation between the constituent tuffs, but flow thickness varies significantly (Figure 11) and some flows contain moderately smoky quartz while quartz is clear in others, likely indicating variation in the U composition of the magma chamber with time. In addition, pumice is light pink in some flows, indicating relatively elevated eruption temperatures, while pumice is white–light grey–light tan in others (Figure 11).

Most flows are pumice-rich, particularly at middle to upper levels (e.g. sample 12JLS202; Figure 12B). Pumice lumps are typically ashy and white, light gray, light tan, or light pink in color and often form moderately flattened ovoid shapes (e.g. 10JLS06A) that range in size from <1–20 cm and weather out in negative to positive relief (Figure 12A–D). In thin section (Figure 13A–D), typical poorly welded pumice lumps (e.g. 10JLS06A) are crystal-rich and contain ~35% phenocrysts, ranging from <0.1–8 mm, of quartz (~20% of phenocrysts), sanidine (~22%), biotite (~25%), plagioclase (~30%), and minor green–brown hornblende (~3%).

By phenocryst content, this tuff is a rhyodacite. The groundmass is composed of microcrystalline plagioclase (lath-shaped to nearly equant), minor biotite, and glass displaying aligned flow textures. Biotite phenocrysts are generally euhedral, display very minor to no textural evidence of resorption, and range from weakly to strongly aligned, depending in part on the degree of welding. Biotite phenocrysts are occasionally kinked around other phenocrysts. Quartz phenocrysts are large and euhedral to subhedral but are typically fractured.

In thin section, the tuff of Dixie Creek has characteristic clusters of sometimes complexly zoned plagioclase (up to ~1 cm). These phenocryst clusters are distinct from the simply zoned and generally monocrystalline plagioclase typically observed in the tuff of Robinson Mountain. Similar clusters of zoned plagioclase are observed in thin section in the most common type of subvolcanic intrusions and rhyolite domes or flows in the study area, suggesting a shared magmatic source that is somewhat distinct from the otherwise compositionally similar tuff of Robinson Mountain.

Some flows, particularly at lower to middle stratigraphic levels, contain minor amounts of pumice having different composition and appearance. One less common pumice type is medium grey and has distinct fibrous or "papery" texture, unusually fine grain size, and abundant aligned biotite (12JLS211). Most phenocrysts of this "papery" pumice type are $\leq$200 μm and consist of quartz (occasionally resorbed and sometimes as large as 2 mm), plagioclase (mostly fresh; some zoned; one phenocryst was observed with a thick rim of hornblende), biotite (generally fresh), sanidine (fresh and sometimes zoned), and rare green hornblende (Figure 13E–G). Pores are smaller (<200 μm) than in the more common white–light grey pumice, and both biotite and the glassy matrix are strongly aligned. By geochemistry, this pumice type is transitional between trachydacite and dacite but only slightly less alkali and silica rich than the more common white to light-grey pumice (Figure 10).

A third type of pumice is medium grey in color, rich in hornblende and biotite, and also unusually fine-grained (12JLS210; Figure 12D). In thin section, this pumice type is unusually rich in euhedral brown hornblende (~35% of phenocrysts; up to ~1 mm) and moderately aligned biotite (~25%), with euhedral sanidine and plagioclase making up most of the remainder of phenocrysts (Figure 13H–I). Quartz is a minor phase, but rare large (~1 mm) shattered and embayed phenocrysts are present and are often at the margins of pores, suggesting that their origin may be from the surrounding more quartz rich tuff. Other than quartz, the only phenocrysts >1 mm are heavily resorbed plagioclase crystals

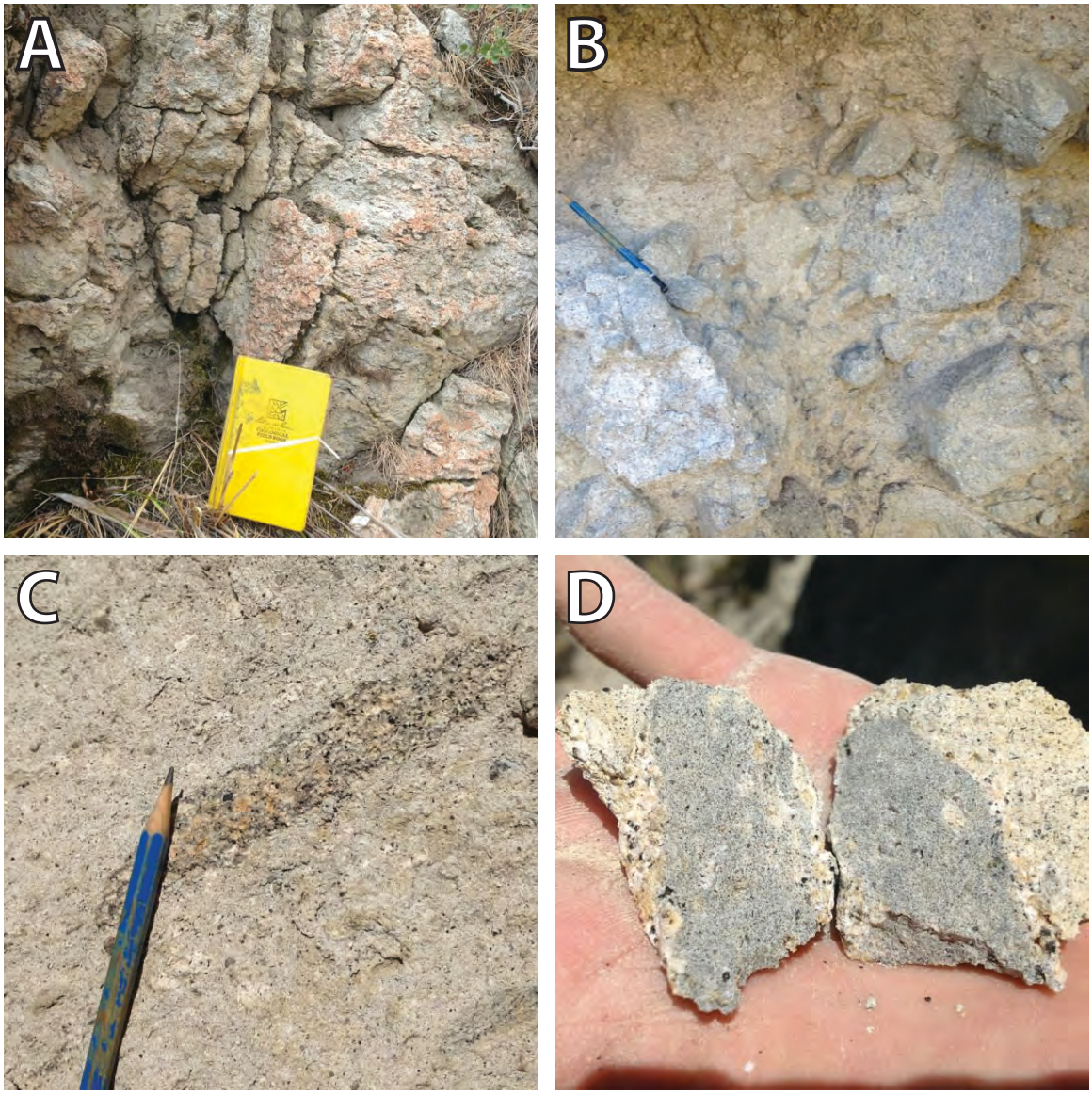


Figure 12: Photographs of the tuff of Dixie Creek. (A) Resistant, vapor-phase altered cap of one flow, with flattened pumice eroding in negative relief. (B) Ashy, poorly welded part of one flow, with pumice and lithics eroding in positive relief. This is the characteristic appearance of the lower parts of thick flows. (C) Example of fiamme in more densely welded part of a flow. (D) Example of fine-grained, medium grey, biotite- and hornblende-rich pumice (e.g. sample 12JLS210) occasionally found as a minor component in some flows. This type of pumice contrasts with the typical light grey–white, ashy, crystal-rich pumice characteristic of the tuff of Dixie Creek (e.g. sample 10JLS06A). A third kind of pumice that is fine-grained, has medium grey color, contains aligned biotite, and has a "papery" texture (e.g. sample 12JLS211) is not displayed here.

Figure 13: Photomicrographs of the tuff of Dixie Creek. (A) A typical light grey pumice lump containing quartz (qtz) and biotite (bt) phenocrysts (sample 10JLS06A), PPL. (B) Closer view of sample 10JLS06A, showing weak eutaxitic texture with biotite and quartz phenocrysts, PPL. (C) Plagioclase (pl) with sieved inner zone and small crystals of plagioclase within sieved areas in typical ashy, white pumice (10JLS06A), XPL. (D) Typical ashy, white pumice (10JLS06A) with fresh (NW corner) and sieved (center) plagioclase, XPL. (E) Aligned, finer-grained biotite with sanidine and plagioclase in medium grey "papery" pumice (12JLS211), XPL. Southwest corner is normal, coarser-grained matrix of tuff of Dixie Creek, outside the pumice. (F) Reaction rim around a rare large plagioclase phenocryst in medium grey, fine-grained "papery" pumice (12JLS211), XPL. (G) Additional view of fine-grained, medium grey "papery" pumice (12JLS211), XPL. Moderately aligned orange crystals are biotite; grey crystals are plagioclase and sanidine. (H) Matrix of a third type of pumice found in some ignimbrites of the tuff of Dixie Creek, which is medium grey and fine-grained (12JLS210), XPL. Phenocrysts are mostly hornblende (hbl), biotite, plagioclase, and sanidine. (I) Large zoned and resorbed plagioclase phenocryst in the rare medium grey, fine-grained, hornblende and biotite rich pumice type (12JLS210; "dark pumice"), XPL. (J) Cross-bedded sedimentary rock between ignimbrites that may represent a base surge deposit (sample 12JLS189), XPL. Mostly angular grains of resorbed and unresorbed quartz, as well as plagioclase, sanidine (s), and biotite, are visible. (K) Pumice taken from a welded portion of the uppermost exposed flow (10JLS05), PPL. (L) Resorbed quartz crystal in a pumice taken from the uppermost exposed flow (10JLS05), XPL.

that are typically situated near vesicles. By geochemistry, this pumice type is more mafic, with a composition transitional between trachydacite and trachyandesite (Figure 10). All three types of pumice occur together in some flows (Figure 11).

A poorly consolidated, cross-bedded, crystal-rich sandstone is observed between two ignimbrites near stratigraphically low parts of the tuff of Dixie Creek (12JLS189). Clasts of siltstone and felsic volcanic rocks are present in small amounts and rarely exceed 5 mm. In thin section, poorly sorted angular grains (average ~0.5 mm) are almost entirely composed of well preserved crystals having nearly the same composition as the surrounding tuff of Dixie Creek, including quartz, sanidine, plagioclase, biotite, and green-brown hornblende (Figure 13J). The matrix (10%) is composed of clay- and silt-sized particles, and an additional ~5% is pore space. The cross-bedding, very high proportion of angular crystals, and relative scarcity of matrix material support the interpretation that these sediments represent a base surge deposit. Another exposure of sedimentary rocks as float between two other ignimbrites (sample 12JLS215) suggests possible base surge deposits at other levels in the section.

**Rhyolite flows and domes (Tiwr)** Rhyolite (by geochemistry) flows and domes locally overlie and underlie the tuff of Dixie Creek but their timing of eruption remains poorly constrained and they may have been erupted in multiple stages. Whole-rock geochemical analysis on vitropheres indicates a peraluminous and calc-alkaline chemistry (Figure 10). Rhyolite flows and domes (Figure 14) are reddish-brown, light grey, medium grey, or red-purple in color and range from glassy and crystal-poor to phenocryst-rich and transitional in some places by phenocryst size (up to ~6 mm) and content with subvolcanic intrusive rocks. Flows and domes commonly display cm-scale flow bands, which form systematic and consistent map patterns in places, but chaotic orientations elsewhere. Phenocrysts include biotite, quartz, and clear feldspars.

At least 7 separate flows or domes are exposed east of Robinson Mountain (Figures 1B and 2), representing a section ~630 m thick (the unreliability of flow banding as a strike and dip indicator in lava flows requires that this thickness is determined from less precise attitude orientations taken on dipslopes). Vitrophere and/or breccia mantle most flows and provide a means for differentiating events. Breccia zones contain angular clasts up to ~1 m, typically resembling the surrounding rhyolite. Vitropheres are usually flow-banded and range from vitreous black to devitrified (microcrystalline) white, light grey, or dusty purple in appearance.

In thin section (sample 10JLS13, a vitrophere), fractured sanidine, quartz, plagioclase, and biotite phenocrysts (Figures 15A–B) comprise ~5% of this sample, but phenocryst content is variable. Where glass is unaltered, flow banding is visible as trails of dark inclusions (Figures 15A–C).

### Thin Eocene sedimentary horizons (Ts)

Thin sandstone, siltstone, and shale layers (Ts) are locally exposed between the Dixie Creek tuff cooling units and overlying rhyolite domes, as well as in horizons within the overlying rhyolite (Figure 2). These horizons, which are typically 20–50 m thick, are light grey to light yellow and poorly consolidated, forming crumbly, rounded outcrops.

Strong layering and moderate sorting differentiate these sediments from the tuff of Dixie Creek, which often has similar mineralogy and appearance. The sediments generally contain clear quartz ($\leq$4 mm) and biotite, as well as ashy, light grey to light yellow pumice that appears to represent air fall and is preferentially concentrated in some layers. Some layers are weakly cross-bedded but the intact pumice and general absence of cross-bedding in others suggest intermittent shallow lacustrine and fluvial environments. This indicates that

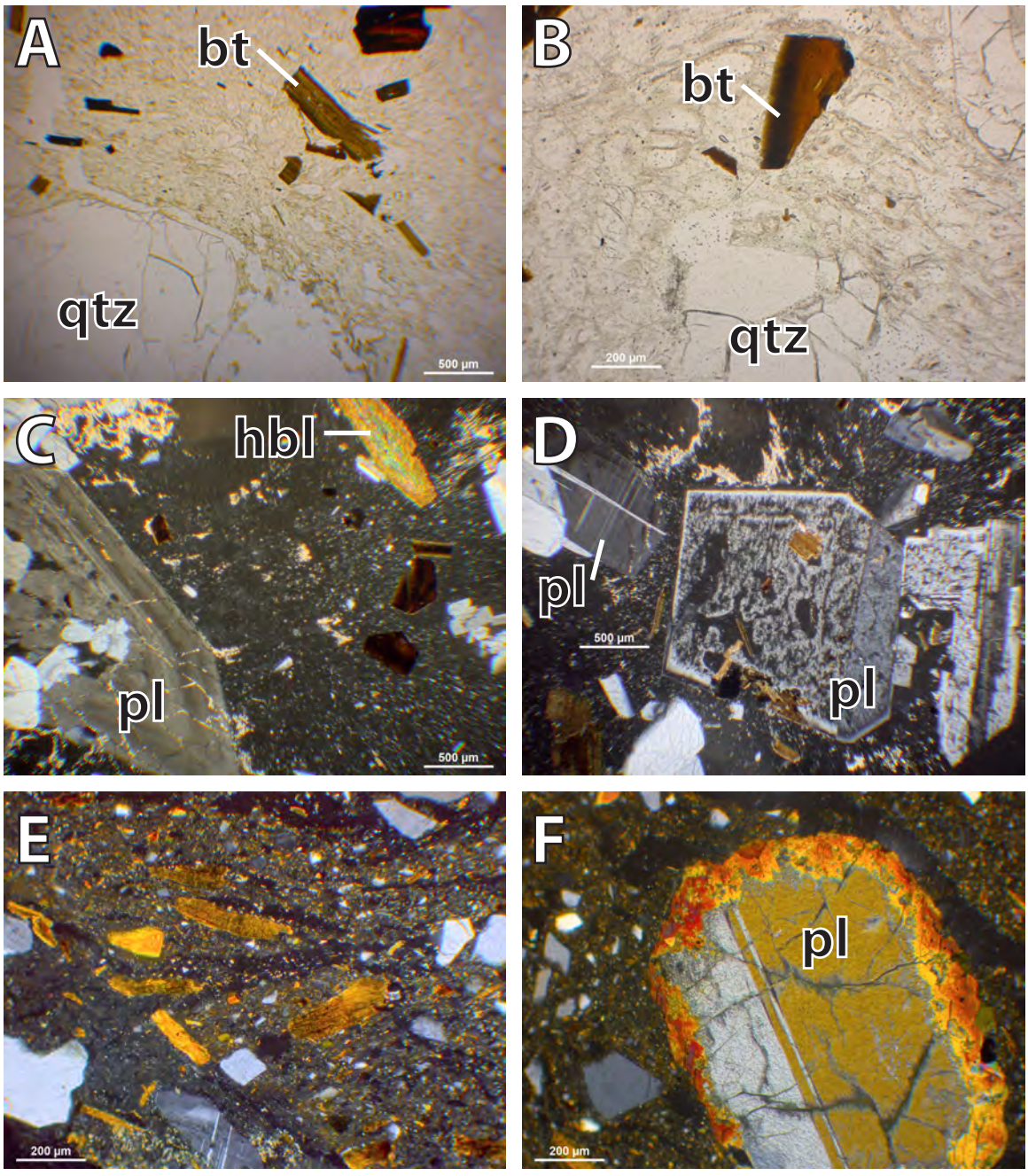
A
bt
qtz
500 µm
B
bt
qtz
200 µm
C
hbl
pl
500 µm
D
pl
500 µm
pl
E
200 µm
F
pl
200 µm

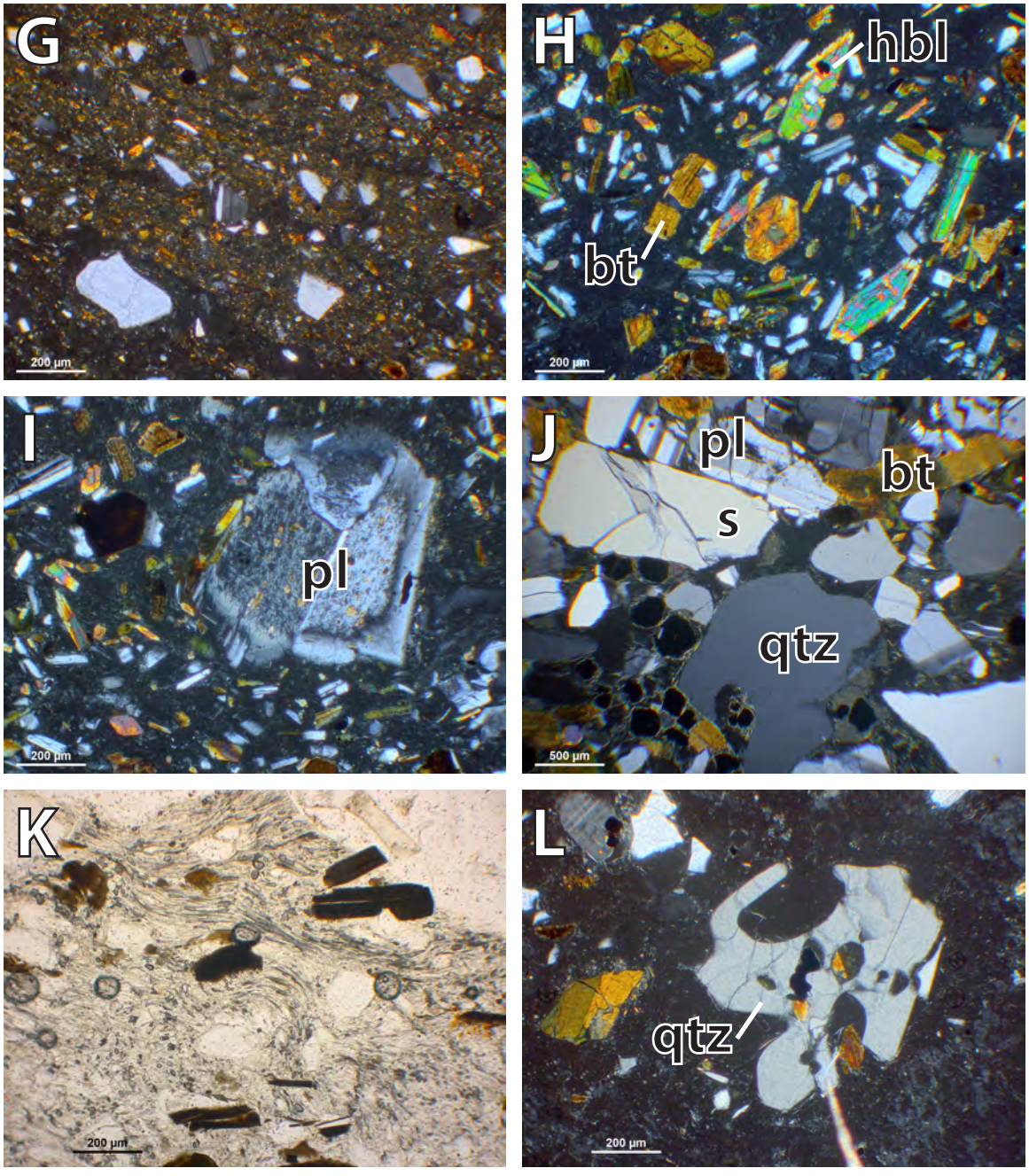
G
200 µm
H
hbl
bt
200 µm
I
pl
200 µm
J
pl
bt
s
qtz
500 µm
K
200 µm
L
qtz
200 µm

Figure 14: Photograph of a typical rhyolite flow (Tiwr) northeast of Robinson Mountain. Note flow banding.

shallow, isolated, and short-lived lakes may have developed at some points during eruption of the tuff of Dixie Creek. In thin section, sample 12JLS130 is composed of crystals of plagioclase, quartz, sanidine, biotite, and green hornblende (Figure 15D).

Other tuffaceous sedimentary rocks are exposed in less clear contact with volcanic and subvolcanic rocks. A bedded, light gray, very poorly sorted tuffaceous rock resembling the tuff of Dixie Creek in color and mineralogy is exposed in one large outcrop (>60 m stratigraphic thickness) west of Cedar Ridge but mostly southeast of the main exposures of the tuff of Dixie Creek (Figure 1; 40.405226°N, 115.865007°W, WGS84). Based on map relations, these sedimentary rocks may represent sediments rafted above felsic lava flows and subvolcanic intrusions; alternatively, they could represent sediments deposited in local paleovalleys by fluviolacustrine or mass wasting processes.

A sample of these deposits (12JLS161) contains angular clasts of crumbly, very crystal-rich, light grey volcanic rocks that are in some cases nearly indistinguishable from the matrix. In thin section, it is mineral-rich (~25%), containing large ($\leq$5 mm) clusters of complexly zoned plagioclase, occasionally resorbed quartz (<4 mm), fresh biotite containing abundant accessory zircon, and green hornblende (Figure 15E). The matrix is composed of aligned and weakly devitrified glass.

Detrital U-Pb LA-ICP-MS geochronology of zircons provides a maximum depositional age of 37.7 ± 0.3 Ma (Lund Snee, 2013), essentially contemporaneous with the tuff of Dixie Creek. Sample 12JLS161 lacks Paleozoic grains but has peaks at 1.26 Ga, 1.41 Ga, 1.73 Ga, and 2.26 Ga, most of which were obtained on inherited cores and thus clearly do not represent a local sedimentary source. They instead provide valuable information about the age of rocks and the nature of the deep crust in the magmatic source region.

Further north of this exposure of Eocene sedimentary rocks, additional Eocene sedimentary rocks are exposed in uncertain contact with volcanic and subvolcanic rocks of the Robinson Mountain volcanic field, and comprise white, bedded sandstones rich in biotite crystals. In thin section, these sandstones (sample TIWB-1) are moderately sorted and composed mostly (~90%) of subrounded–subangular clasts, with minor plagioclase, quartz, sanidine, biotite, and green hornblende (~2%), with a matrix of brown clay minerals (~8%) (Figure 15F). Clasts are predominantly one type of volcanic rock having aligned plagioclase and biotite microlites in a glassy groundmass with occasional phenocrysts of plagioclase and quartz. Rarer clasts include volcanic rocks having a trachytic, holocrystalline groundmass composed entirely of plagioclase microlites and no phenocrysts, as well as minor siltstones and devitrified felsic volcanic rocks resembling rhyolite lavas associated with the tuff of Dixie Creek. A maximum depositional age of 37.3 ± 0.1 Ma was determined for TIWB-1 (Figure 2). The ~37 Ma zircon population is likely derived from the underlying tuff of Dixie Creek or from locally exposed subvolcanic intrusions.

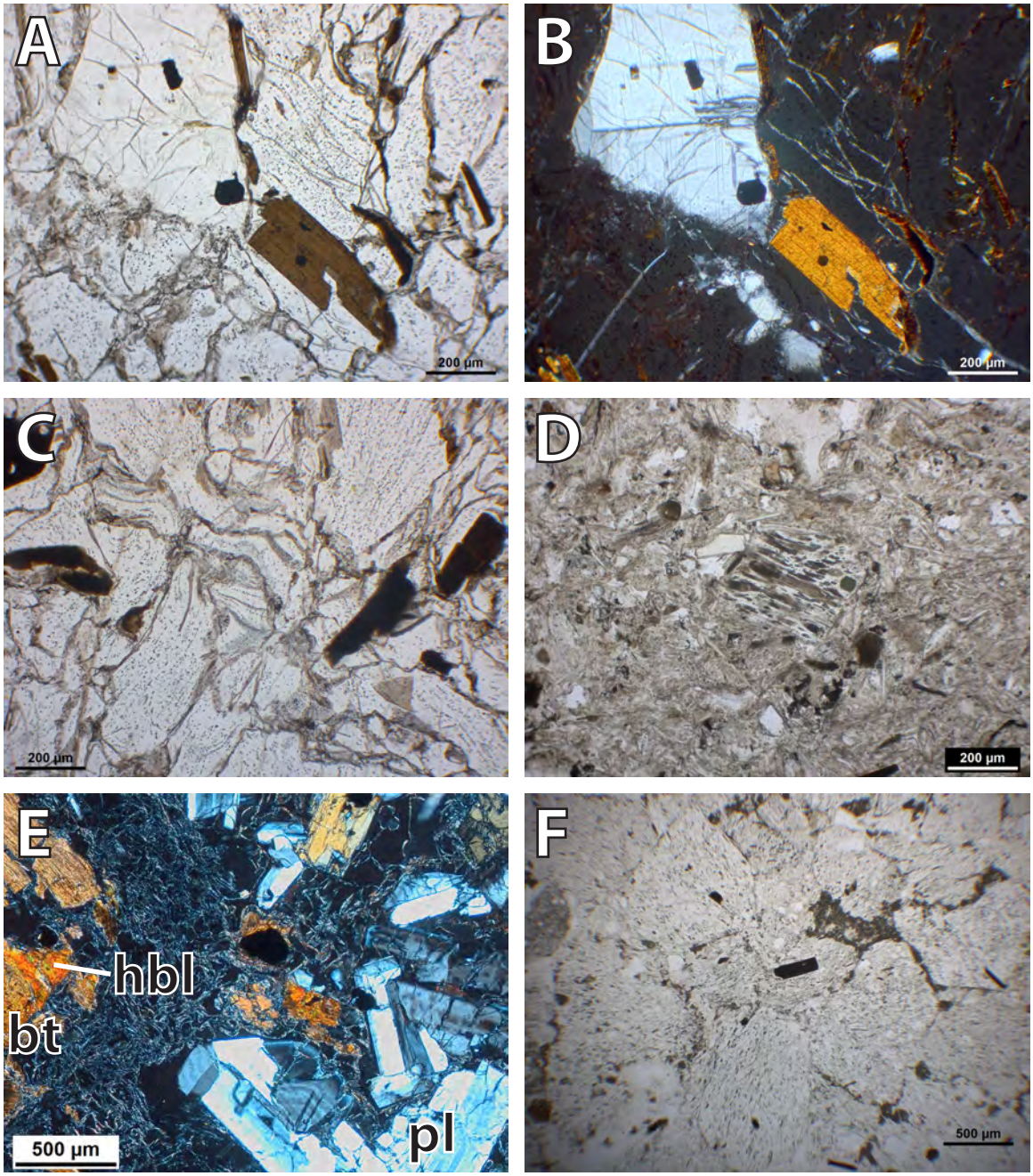


Figure 15: (A) Photomicrograph of a sample from a rhyolite dome containing plagioclase and biotite phenocrysts in a weakly devitrified groundmass (sample 10JLS13), PPL. (B) Same view as (A) in crossed polars. (C) Photomicrograph of glassy groundmass of rhyolite vitrophere, with dark biotite phenocrysts (sample 10JLS13), PPL. (D) Photomicrograph of sedimentary rock collected north of Robinson Mountain, stratigraphically above the tuff of Dixie Creek (sample 12JLS130), PPL. (E) Tuffaceous sedimentary rocks (unit Ts) having clusters of plagioclase ("pl;" E side of image) characteristic of the tuff of Dixie Creek in a glassy matrix, with biotite (bt), hornblende (hbl), and opaque oxide phenocrysts (sample 12JLS161), XPL. (F) Volcanic clast-rich pebbly sandstone (unit Ts; sample TIWB-1), PPL.

### Subvolcanic intrusions (Tsvi)

Rhyolitic (by geochemistry), weakly calc-alkaline subvolcanic intrusions are voluminous in the study area. In most exposures, these rocks are porphyritic and typically light to medium grey, medium brown, rust-red, or purple in outcrop, and contain large sanidine phenocrysts and euhedral biotite. Most notably, they form the tall edifices of Robinson Mountain (e.g. sample JLS-PLUG-1) and Squaw Mountain (e.g. sample 11JLS104; Figure 1B), which were likely large volcanic necks that intruded local ignimbrites.

Subvolcanic intrusions are often flow-banded and are transitional in some cases with rhyolite domes and flows, making the two rock types occasionally difficult to distinguish. Subvolcanic intrusions were identified in the field on the basis of their large sanidine phenocrysts (usually >0.8 cm) and high crystal content. These intrusions appear to mostly post-date and intrude other Eocene volcanic rocks of the Robinson Mountain volcanic field, including the tuff of Dixie Creek and Robinson Mountain. In one location, however, a brown–purple–red subvolcanic intrusion may be approximately synchronous with voluminous rhyolite flows to the east of Robinson Mountain that are exposed near the tuff of Dixie Creek. In this case, the intrusive rocks are exposed in a steeply east-dipping tabular body (e.g. 40.410014°N, 115.895854°W, WGS84) with north-northeast-trending map pattern that is in contact with the east side (bottom) of gently west-dipping rhyolite domes and flows. These intrusive rocks may represent a partially exhumed conduit that fed eruption of the domes. A sanidine $^{40}Ar/^{39}Ar$ age of 37.51 ± 0.38 Ma was previously obtained from this intrusion in the map area (sample 98-DJ-31 of Ressel and Henry, 2006).

A single exposure of moderately west-dipping yellowish-tan claystone (40.402144°N, 115.894151°W, WGS84) in possible contact with the bottom (eastern side) of the tabular body (but possibly surrounded by subvolcanic intrusive rocks) has not been dated. However, its stratigraphic position supports the inference that it is a thin, interbedded or rafted sedimentary rock horizon (Ts) of likely Eocene age associated with the Robinson Mountain volcanic field, and therefore younger than the Elko Formation, as it was originally mapped by Smith and Ketner (1978).

All subvolcanic intrusions are likely younger than the Eocene tuff of Dixie Creek, based on map relations, geochronologic analysis of some intrusions (Lund Snee, 2013), and very similar mineral assemblage to the Eocene volcanic rocks. U-Pb zircon ages were obtained from a subvolcanic intrusion immediately east of Robinson Mountain (sample 10JLS11A), which returned an age of 36.8 ± 0.3 Ma, and a subvolcanic intrusion on Squaw Mountain (11JLS104), which returned an age of 37.6 ± 0.7 Ma (Figure 1). These ages are within error of one another but could equally indicate protracted intrusion of these mineralogically and texturally similar intrusive rocks.

In thin section of a characteristic sample of subvolcanic intrusive rocks (10JLS11A), phenocrysts (~35%) comprise plagioclase (~50%), biotite (25%), sanidine (18%), quartz (10%), and green hornblende (2%). Disequilibrium textures are evident in most phenocryst phases. Weak reaction rims are observed around quartz and sanidine phenocrysts but the interiors are generally fresh (Figure 16A). Reaction rims typically mantle hornblende and biotite, and the interiors are sieved and altered (Figure 16B). Plagioclase phenocrysts have typically experienced preferential alteration of what are likely relatively Ca-rich zones (Figure 16C).

A vaguely flow-banded, strikingly white subvolcanic intrusion (Tsviw) is exposed in a small area at the northwest corner of the field area (12JLS149), representing a notable exception to the generally monotonous character of these rocks. At that location, map patterns indicate that this unit forms a tabular, nearly vertical feature that is likely a dike. The unit contains large (≤5–6 mm) smoky quartz, abundant biotite, and clear feldspar. In thin section, the white subvolcanic intrusion (Tsviw) is distinguished from the more common brown–purple–red–grey subvolcanic intrusions (Tsvi) by higher quartz content (~40% of phenocrysts and typically embayed and surrounded by reaction rims) and less biotite (~10% of phenocrysts), and having a glassier matrix that contains finer and more elongate microlites (Figure 16D).

Another exception to the general brown–purple–red–grey appearance of subvolcanic intrusions is a flow-banded, light grey to light pink subvolcanic unit that weathers to an unusually light rust-red color, is devitrified in places, and is exposed only in a small area west of Robinson Mountain (12JLS119). This subvolcanic intrusion (Tsvip) contains biotite, large (≤6 mm) smoky quartz, and large feldspar phenocrysts (some >6 mm). In thin section (Figure 16E–F), it is very crystal-rich (~40%). Quartz (20% of phenocrysts) is usually round and resorbed but occasionally euhedral (hexagonal). Biotite (10%) is euhedral but red and somewhat altered, and resembles the large amount of oxyhornblende (20%) in color. Sanidine content is low (~5%) and plagioclase phenocrysts (45%) are often zoned, are clustered, and range from strongly resorbed to fresh. The groundmass is composed mostly of glass with lesser amounts of very fine plagioclase microlites. Pore space is unusually abundant and occasionally surrounded by devitrified areas of groundmass, and suggests emplacement very near the surface, perhaps near a vent.

Additional subvolcanic intrusive rocks including dikes were mapped as "silicic intrusive rocks" (Ti) by Smith and Ketner (1978) and are exposed in the Bailey Mountain quadrangle at the southwestern corner of the map area (e.g. 40.373013°N, 115.968833°W, WGS84), and in the western part of the Robinson Mountain quadrangle. These rocks intrude Paleozoic rocks of the Piñon Range.

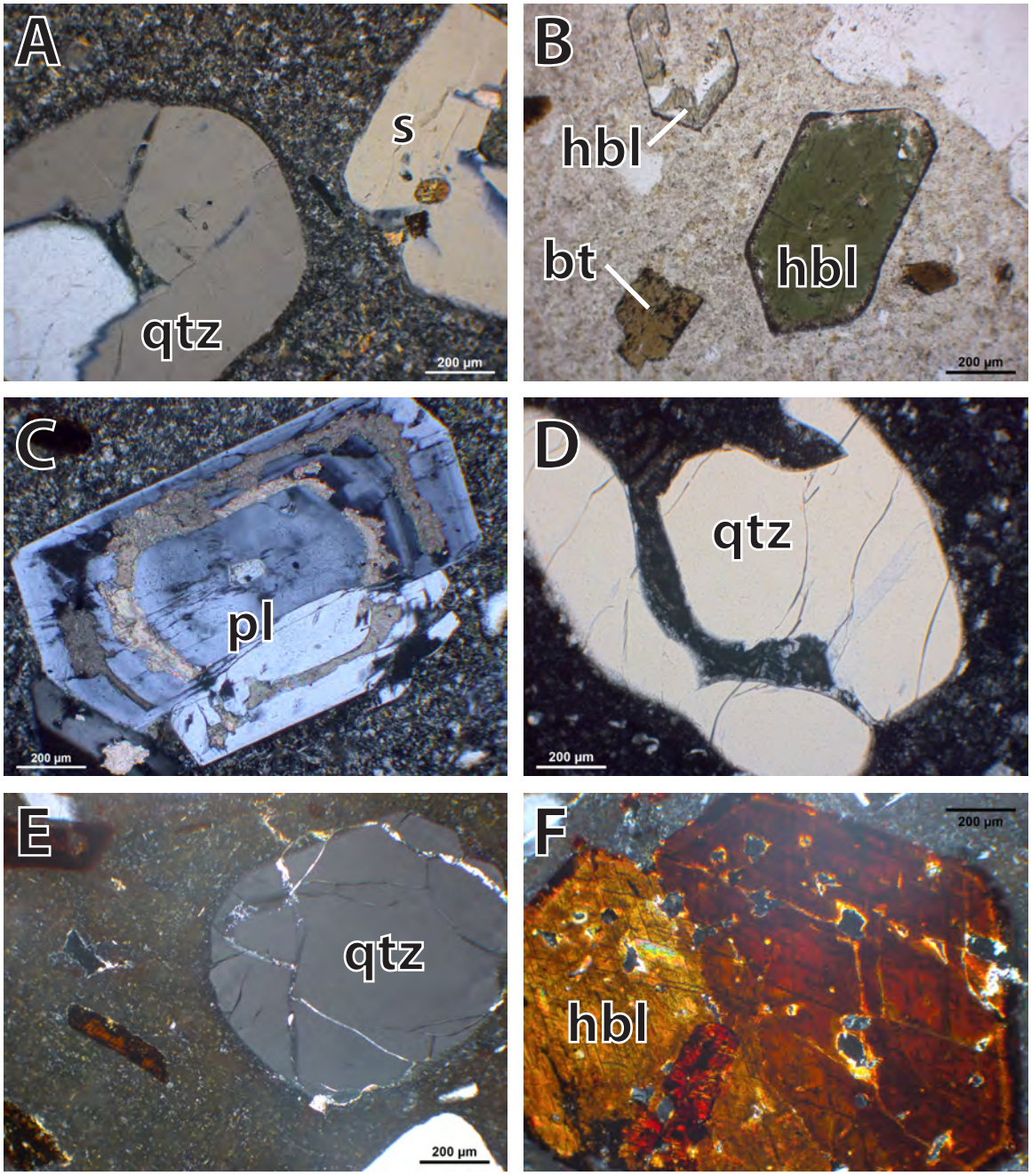


Figure 16: Photomicrographs of subvolcanic intrusive rocks (Tsvi). (A) Reaction rims around quartz (qtz) and sanidine (s) phenocrysts in a typical subvolcanic intrusion (sample 10JLS11A), XPL. (B) Resorption textures (reaction rims and sieved interiors) affecting green hornblende (hbl) and biotite (bt) in a typical subvolcanic intrusion (10JLS11A), PPL. (C) Calcite replacement of resorbed zones in a large plagioclase phenocryst (pl), surrounded by microcrystalline matrix in a typical subvolcanic intrusion (10JLS11A), XPL. (D) Resorbed quartz and microcrystalline groundmass in a tabular, strikingly white subvolcanic intrusion (Tsviw) sampled at the northwest corner of the map area (12JLS149), XPL. (E) Fractured quartz and smaller biotite phenocrysts in microcrystalline groundmass of a light grey to light pink subvolcanic intrusion (unit Tsvip, sample 12JLS149), XPL. (F) Light grey to pink subvolcanic intrusion (unit Tsvip, sample 12JLS149), XPL. View is of a resorbed (sieved and with reaction rims) oxyhornblende crystal.

## Cenozoic mafic–intermediate composition rocks

### Aphanitic basaltic andesite flows (Tba)

Platy, vesicular ($\leq$1 cm openings), dark grey to black, nearly aphanitic lava flows are exposed to the northwest of Robinson Mountain, where they overlie reddish-brown to medium-grey rhyolite flows (Figure 2). Smith and Ketner (1976) assigned a Late Miocene age to these flows on the basis of 1) their stratigraphic position above the tuff of Dixie Creek, and 2) the lack of obvious clasts of these rocks in the Humboldt Formation to the east. Dates for andesite flows outside the study area, in the Sulphur Spring Range and the Elko Hills, range from ~31–38 Ma (Solomon et al., 1979; Haynes, 2003; Ryskamp et al., 2008). It is unclear from map relations whether the basaltic andesite (Tba) in the map area is of comparable age to the tuff of Dixie Creek (i.e. 36–37 Ma) or significantly younger (i.e. Late Miocene), but there is little to no angular unconformity separating these units, which suggests that they are older than Middle Miocene age. The difficulty determining dip of these flows also contributes to uncertainty about the thickness estimate of at least 150 m for 2 or more flows.

In thin section, a sample (12JLS124) of this unit is composed of a hypocrystalline groundmass of weakly aligned plagioclase laths (avg. ~150 μm long) with minor (~5%) phenocrysts (mostly $\leq$1 mm). Phenocrysts include clinopyroxene (often occurring in clusters), plagioclase with preferentially altered interiors, and altered red biotite (Figure 17A). Differences in texture, grain size, and mineralogy are observed in thin section between different samples, likely reflecting the exposure of multiple flows in the map area. A different sample (10J3.5) contains sparse phenocrysts of resorbed quartz up to ~3 mm with alteration rims, clusters of clinopyroxene, and extensively altered sanidine and biotite in a trachytic groundmass of much smaller plagioclase laths (avg. ~50 μm) and opaque oxides (Figures 17B–D).

### Aphanitic basaltic trachyandesite intrusion (Tbta)

A small ($\leq$0.2 km$^2$), black, isolated intrusion of basaltic andesite composition (by whole-rock geochemistry), is exposed in the Robinson Mountain quadrangle (e.g. 40.411642°N, 115.965216°W, WGS84), at the western edge of the map area, to the west of the east-dipping normal fault system that bounds the Piñon Range. In thin section (sample 12JLS125; Figures 17E–F), this intrusion is composed of a holocrystalline groundmass of interlocking plagioclase (~49%), altered green hornblende (~30%), biotite (~4%), and opaques (~2%). A portion of the reported plagioclase may be quartz but the grain size of these crystals is too small to obtain an optic axis figure. The rock has been extensively replaced by calcite (~15% of total rock). The age of this intrusion is uncertain but its similar mineralogy and texture to the nearby aphanitic basaltic andesite flows (Tba) suggests that it may be of similar age to those flows.

## Oligocene tuff of Hackwood Ranch (Tthr)

### Ignimbrites

The tuff of Hackwood Ranch comprises three (or more) cooling events of strongly cliff-forming, poorly welded, reddish-brown, tan, or green ignimbrite (Figures 2 and 18A). It was previously named the "tuff of Hackwood" by Palmer et al. (1991), but our new name better reflects its exposure near Hackwood Ranch (Figure 1B).

The tuff of Hackwood Ranch is crystal poor and contains only small phenocrysts ($\leq$3 mm) of mostly biotite that are visible in hand sample. It is pervasively silicified and typically has conchoidal fracture and vitreous luster that disguises vitreous silicate phenocrysts in hand sample. Eruption occurred at ~31.1 Ma, which is within the age span of caldera eruptions near the Desatoya and Clan Alpine Mountains, central Nevada (Figure 1A), some of which were deposited hundreds of kilometers from their eruptive centers (Faulds et al., 2005; Henry et al., 2012; Henry and John, 2013). The tuff of Rattlesnake Canyon appears to be the most correlative tuff, based on its similar 31.2 Ma eruptive age (Henry and John, 2013). If instead erupted from nearby, the tuff of Hackwood Ranch may represent the last eruptions of the general Robinson Mountain volcanic field.

In thin section, some pore space is filled with secondary microcrystalline quartz (Figures 19A–B). The matrix is composed chiefly of moderately aligned glass shards, together with secondary microcrystalline quartz. Rare lithic fragments (5%) are siltstone or volcanic rocks resembling the underlying tuff of Dixie Creek and rhyolite flows and domes. Phenocrysts are $\leq$3 mm and include quartz (~5% of phenocrysts), sanidine (>50%), plagioclase (~30%), and biotite (~15%), which is occasionally sieved and embayed. Some plagioclase is heavily resorbed but most is fresh. By phenocryst content, this tuff is transitional between quartz latite and latite, but resorption textures in some phenocrysts suggest that they may be xenocrystic. Whole-rock (sample 11JLS105) and pumice-only (sample HACK-1) geochemical analysis indicates that this tuff is a high-silica rhyolite (Figure 10), but outcrop and thin section evidence for secondary silicification suggests that it may have artificially high silica (and artificially low alkali) content.

### Underlying sandstones

Thin (~35 m), poorly consolidated, cross-bedded silty sandstone and pebble conglomerate underlie the ignimbrites (Figure 2) and are mapped together with the tuff of Hackwood Ranch due to map resolution and their infrequent exposure. Clasts, including crystals, form ~75% of the rock, and are angular and up to 2 cm (Figures 18A–C). In thin section (sample 10JLS08), clasts consist of sanidine, plagioclase,

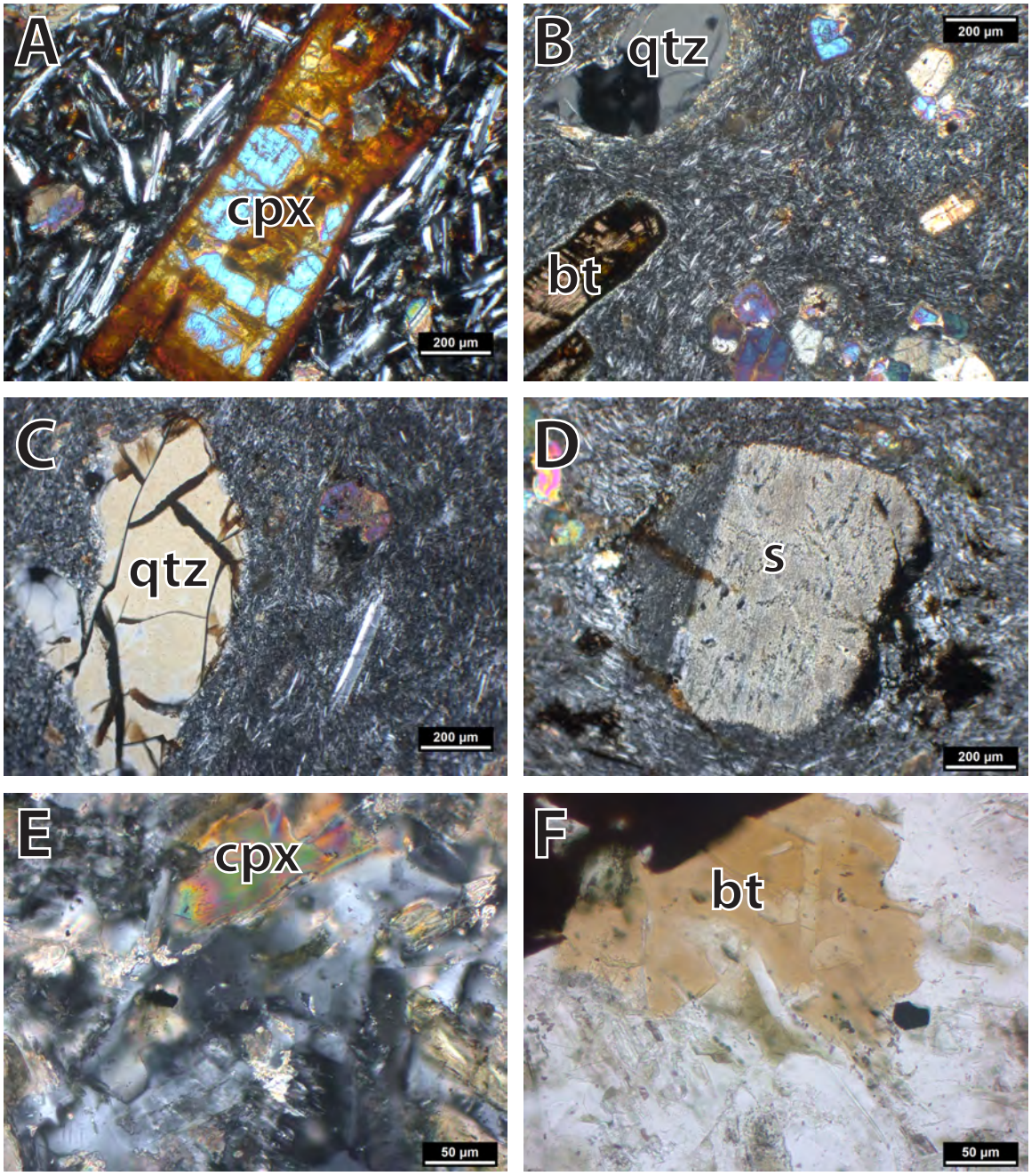


Figure 17: Photomicrographs of mafic-intermediate composition volcanic rocks overlying the tuff of Dixie Creek. (A) Aphanitic black andesite flow (Tba, sample 12JLS124), XPL. The large phenocryst is likely altered clinopyroxene (cpx), in a matrix of glass, plagioclase laths, and smaller clinopyroxene. (B) Aphanitic basaltic andesite flow sampled in a different location (Tba; sample 10J3.5), XPL. The groundmass is finer and visible resorbed phenocrysts include quartz (qtz), clinopyroxene, and biotite (bt). (C) Resorbed quartz (qtz) and fresh plagioclase in a finer-grained aphanitic basaltic andesite flow sampled from the second location (Tba, 10J3.5), XPL. (D) Probable sanidine (s) phenocryst that has been strongly altered (Tba, 10J3.5), XPL. (E) Fine-grained matrix of altered, aphanitic basaltic trachyandesite, showing plagioclase and likely augite (cpx), with brightly colored secondary calcite (sample 12JLS125), XPL. (F) Biotite and opaque crystals in altered, aphanitic basaltic trachyandesite (sample 12JLS125), XPL.

quartz, biotite, hornblende, and occasional pyroxene crystals, as well as lithics of siltstone, felsic pumice, intermediate–mafic composition volcanic rocks containing clinopyroxene (Figures 19C–D), and felsic volcanic rocks resembling the tuff of Dixie Creek and locally exposed subvolcanic intrusions. The remaining matrix material is composed of clay- and silt-size particles, some of which are fine-grained biotite, as well as minor volcanic ash.

A maximum depositional age of 33.9 ± 0.4 Ma was determined from U-Pb detrital zircon analysis of the sedimentary rocks (sample 10JLS08). The ~34 Ma zircon population could represent reworked air fall from the ~33.8 Ma Caetano Tuff or the older and less aerially extensive 34.2 Ma tuff of Cove Mine also erupted from the Caetano caldera ~75 km southwest of the map area (John et al., 2008).

The presence of cross-bedded sandstones between the tuff of Hackwood Ranch and the tuff of Dixie Creek (10JLS08) suggests a fluvial environment between deposition of the tuffs. This, together with the presence of a gentle angular unconformity (~10–15°) that is developed between these sedimentary rocks and the underlying tuff of Dixie Creek (Palmer et al., 1991; Gordee et al., 2000; Lund Snee, 2013), indicates that tilting of rocks to the west-northwest occurred between about 37.3 Ma and 33.9 Ma.

## Other Eocene or Oligocene tuffs or tuffaceous sedimentary rocks (Tt)

Orange-weathering tuffs or tuffaceous sedimentary rocks (Tt) are exposed in a small area (<0.2 $km^2$) at the northern edge of the map area. This unit (samples 11JLS101 and 11JLS102), which is bedded and devitrified and/or significantly hydrothermally altered in places, resembles the tuff of Hackwood Ranch in its low content of crystals (~3%; mostly sanidine, plagioclase, and quartz), pumice (~5%), and lithics (~1%) (Figure 20A). However, it differs from the tuff of Hackwood Ranch by its composition of mostly glass shards, which are weakly to moderately aligned and completely unflattened. Clast alignment, low prevalence of pumice, bedding, and alteration (Figure 20B) suggest a water-laid air-fall tuff or gently reworked terrestrially-deposited air-fall tuff. High amounts of ash shards and sparse pumice and lithics suggest deposition distal from a large silicic eruption. These deposits are not easily correlated with the four main tuffs described here in part because they are exposed in an isolated area. They are therefore mapped as undifferentiated Tertiary tuffs or tuffaceous sedimentary rocks (unit Tt).

## Miocene Humboldt Formation (Th)

Miocene Humboldt Formation (Th) sedimentary rocks in the mapped area were originally divided into a Pliocene Humboldt Group and Eocene Green River Group by Hague and Emmons (1877) and King (1878). The Humboldt Formation name has since been applied to diverse sedimentary rocks of Miocene age deposited in a lacustrine–fluvial environment in northeastern Nevada (Sharp, 1939; Smith and Ketner, 1976; Smith and Howard, 1977; Smith and Ketner, 1978; Solomon et al., 1979; Stewart, 1980; Wallace et al., 2008; Colgan et al., 2010). Sharp (1939) initially measured ~1800 m thickness of this unit east of Huntington Creek (Figure 1B), and noted an upward progression from a lacustrine to fluvial depositional environment.

Smith and Ketner (1978) later restricted the Humboldt Formation to include 560 m of the middle and part of the upper members of Sharp (1939)'s section. Their definition included upper Miocene conglomerate, sandstone, siltstone, and claystone with beds of limestone, tuff, and ash, represented by part of the same type section at the east side of Huntington Creek (e.g. 40.610500°N, 115.691400°W, WGS84), immediately east of the eastern edge of the present study area (Figure 1B). To the west of this type section, in an area including Indian Well and Crane Springs (Figure 1B), Smith and Ketner (1978) mapped a large portion of the present study area as Eocene–Oligocene (Walker et al., 2012, time scale) "Indian Well Formation" sedimentary rocks (Figure 2). Subsequent workers have adopted this naming for those sediments in Huntington Valley (Solomon et al., 1979; Satarugsa and Johnson, 2000; Haynes, 2003; Horton et al., 2004; Horton and Chamberlain, 2006; Chamberlain et al., 2012).

This more recent mapping study, which was supported by detrital zircon and sanidine $^{40}Ar/^{39}Ar$ geochronology as outlined by Lund Snee (2013) and Lund Snee et al. (submitted), found that most of the sediments previously associated with the (now abandoned) "Indian Well Formation" in the study area are significantly younger than that unit and are likely part of the mostly Miocene Humboldt Formation. For this reason the Humboldt Formation has been expanded to include latest Oligocene to Miocene conglomerate, sandstone, siltstone, claystone, marl, and interbedded limestone, ash, and tuff (Figure 2). In general, the Humboldt Formation is characterized by the vitric ash beds (Figure 2).

Our expanded definition for the Humboldt Formation includes strata at the base of this unit (west of Cedar Ridge and Red Spring) that were formerly grouped with the (abandoned) "Indian Well Formation," making the total thickness of the Humboldt Formation ~2130 m (Figure 2). About 1740 m of the total represents the lower and middle parts of the formation that are exposed west of Red Spring and Cedar Ridge. Unlike at Sharp's (1939) type section to the east of Huntington Creek, these newly incorporated Humboldt Formation strata further west generally grade upward from fluvial to lacustrine depositional settings (Figure 1B). About 1100 m of this western section was previously mapped as "Indian Well Formation" sedimentary rocks by Smith and Ketner (1978).

The total thickness of the Humboldt Formation is complicated by open folds and a normal fault system that partly

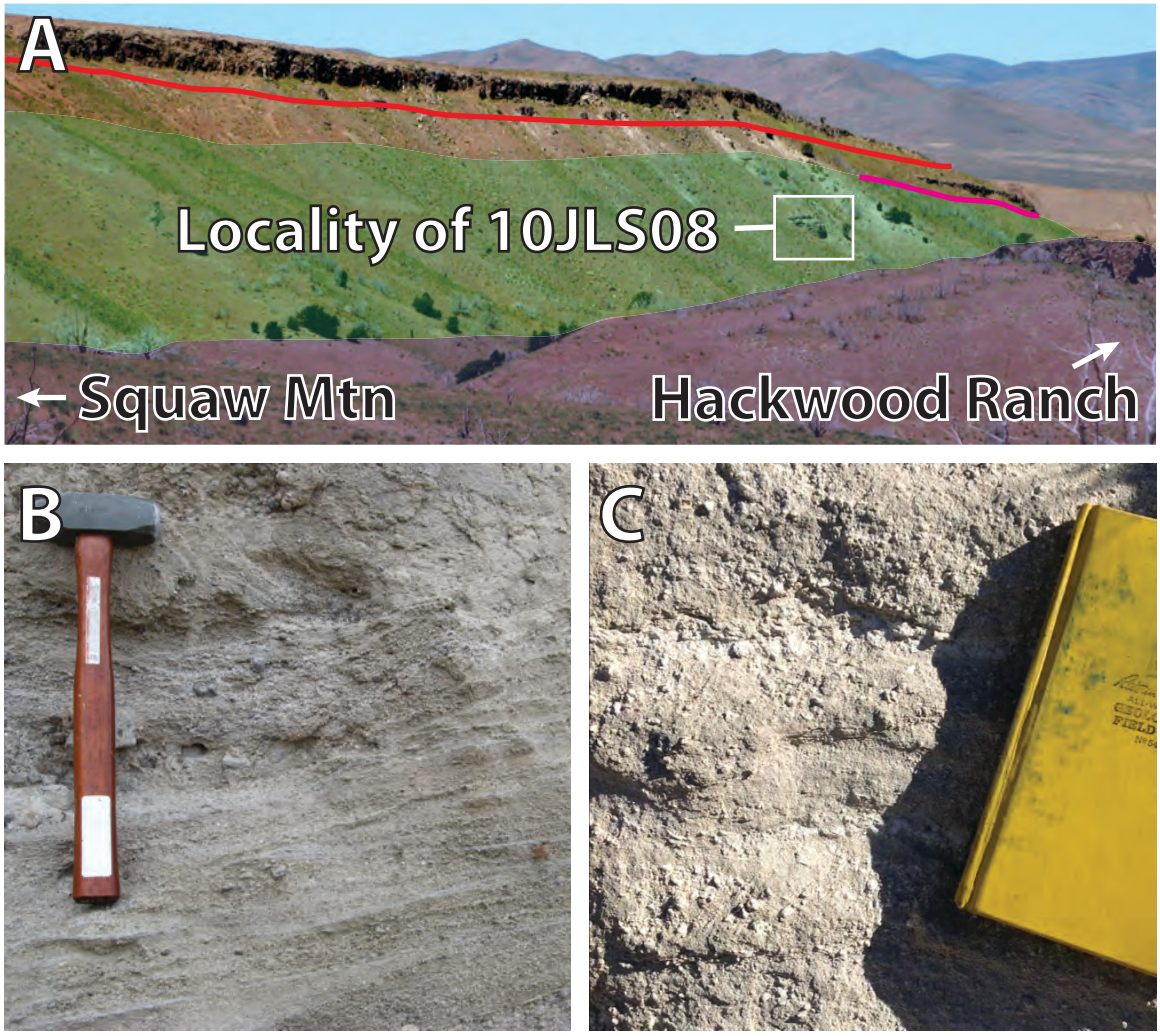


Figure 18: Photographs of the tuff of Hackwood Ranch. (A) View to the west of the tuff of Hackwood Ranch. Red and pink lines mark the approximate bottoms of two flows. Sediments underlying the tuff of Hackwood Ranch — shown in (B) and (C) — are shaded green. The underlying tuff of Dixie Creek (Ttdc) is shaded purple. (B) Cross-bedded pebbly sandstones between the tuff of Hackwood Ranch and tuff of Dixie Creek (e.g. sample 10JLS08). Sample locality indicated by the white box in (A). A gentle angular unconformity separates these sedimentary rocks from the underlying tuff of Dixie Creek (Figure 2). (C) Sedimentary rocks below the tuff of Hackwood Ranch exposed about 1.1 km north of (B).

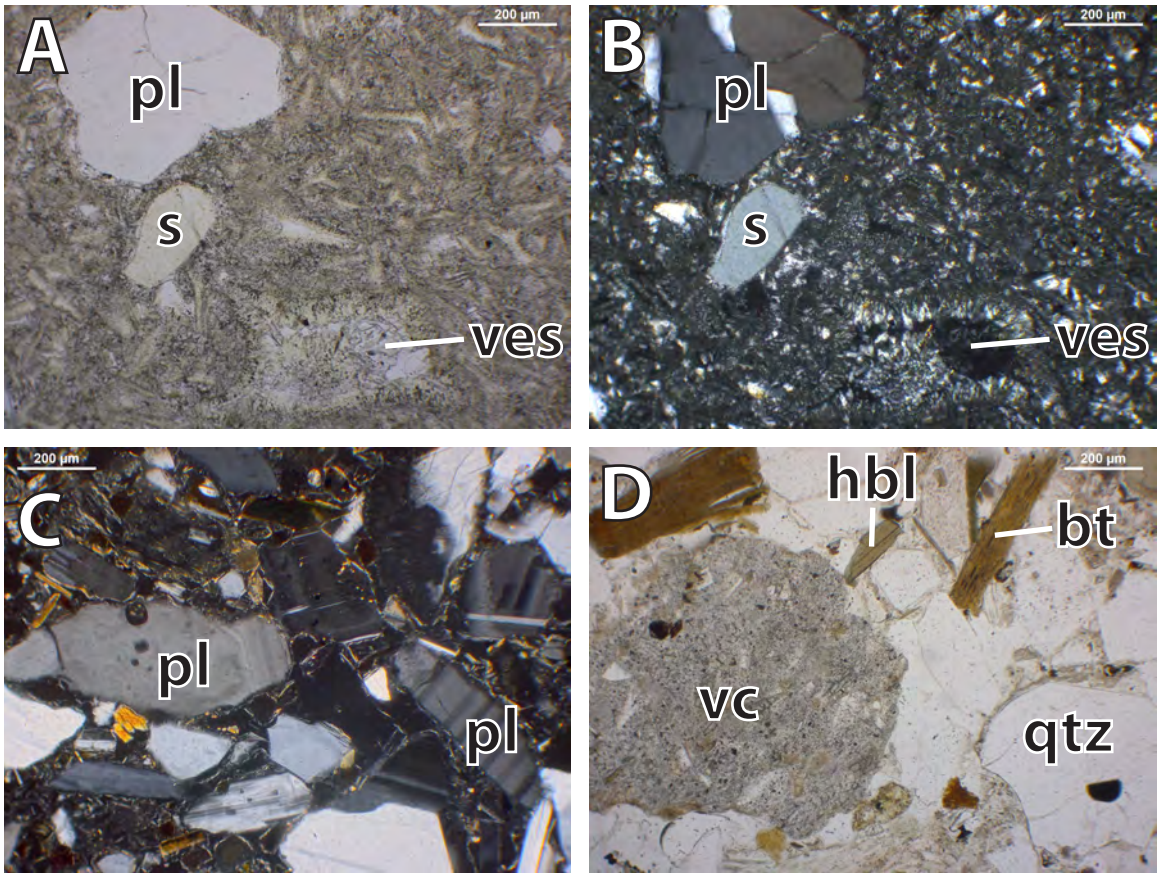


Figure 19: Photomicrographs of the tuff of Hackwood Ranch and underlying sedimentary rocks. (A) Ashy matrix and phenocrysts of plagioclase (pl) and sanidine (s) in the tuff of Hackwood Ranch (sample 11JLS105). (B) Same view as (A) in crossed polars. (C) Pebbly sandstone below the tuff of Hackwood Ranch (sample 10JLS08), XPL. (D) Pebbly sandstone below the tuff of Hackwood Ranch (sample 10JLS08), PPL. A volcanic clast (vc), likely from a subvolcanic intrusion, is on the W side, and quartz (qtz), biotite (bt), and hornblende (hbl) crystals are visible.

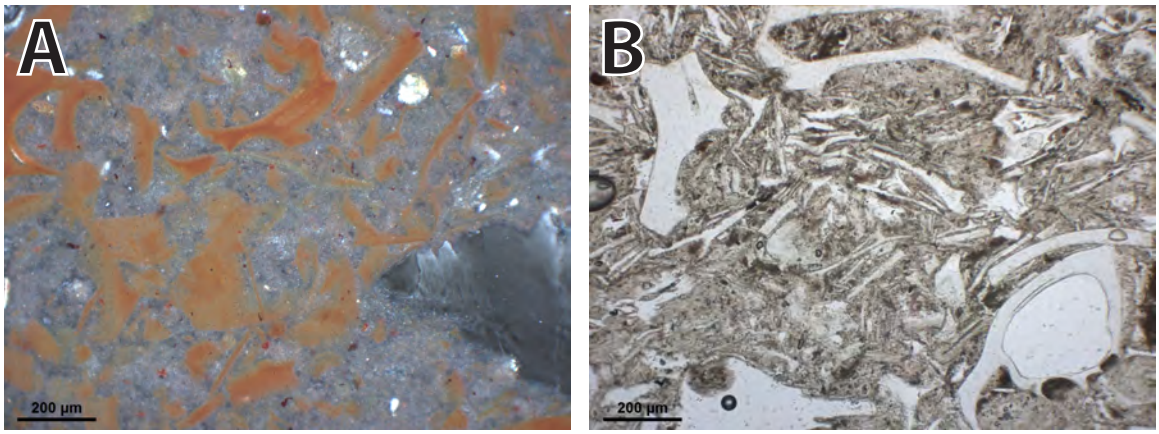


Figure 20: Photomicrographs of Eocene or Oligocene age tuffaceous sedimentary rocks (unit Tt). (A) Altered reddish glass shards, sparse phenocrysts, and glassy matrix in what are likely tuffs or tuffaceous sedimentary rocks exposed at the northern edge of the map area (sample 11JLS101), PPL. (B) Less altered ash and glassy matrix in what may be the same tuffs or tuffaceous sediments as (A) (sample 11JLS102), PPL.

repeat the section, but bedding attitudes and geochronology limit error associated with this measurement (Figure 2). Wallace et al. (2008) estimate that the fault slipped ~700 m and cuts the Humboldt Formation. It is difficult to constrain the amount of offset precisely because movement along this fault system appears to have occurred both during and after deposition of the Humboldt Formation. Older Cenozoic units, including what may be the Eocene Elko Formation, are exposed east of the fault, and the Humboldt Formation is ~1740 m thick to the west of the fault, indicating that the 700 m value is likely a low estimate.

At least 90 m of section overlie the locality of the youngest Humboldt Formation sample analyzed (12HBD09), which is exposed east of the Cedar Ridge fault system, so for these reasons we cautiously add 390 m to the 1740 m measured for the lower part of the section to give a final stratigraphic thickness measurement of ~2130 m in the mapped area. This is probably a minimum value and does not count additional overlying strata that are poorly exposed further east in the map area, nor those exposed east of the map area toward the RMEH (Figure 2).

The Humboldt Formation (expanded) overlies the Oligocene tuff of Hackwood Ranch across a moderate angular unconformity (~30°) that is never directly exposed in the map area (Figure 2). However, a grey tuff resembling the tuff of Hackwood Ranch is exposed ~60 m (map distance) from an outcrop of the basal Humboldt Formation at 40.508581°N, 115.881708°W, WGS84.

The lowest (and furthest west) exposures of the Humboldt Formation in the map area (e.g. 40.508581°N, 115.881708°W, WGS84, sample 12HBD03; 40.492278°N, 115.884230°W, WGS84, sample ELM11-PN19) are pebble conglomerates and poorly sorted, often cross-bedded sandstone and siltstone. Tuffaceous material is present in poorly consolidated pebble conglomerate and sandstone at one exposure of conglomeratic sandstone at the base of the Humboldt Formation (sample ELM11-PN19; 40.492278°N, 115.884230°W, WGS84). At this location, clasts include unflattened, ashy white to light grey tephra ($\leq$2 cm) lacking obvious biotite, as well as sparse subrounded to subangular clasts ($\leq$2 cm) resembling local felsic volcanic rocks. Silt to fine sand layers are situated in a poorly sorted, light grey sandstone.

In a thin section of the sandstone, the unwelded matrix between clasts is composed of ash, pumice, and sparse fine to medium sand grains (Figure 21A). Glass fragments are tightly packed but appear unflattened, and scant material is observed between clasts; minor primary or secondary (possible devitrification) clay minerals surround glass fragments, but little to no calcite is observed. Crystal-poor tephra are unflattened, angular, and strongly vesicular, indicating no welding of the deposit. Grains are mostly single crystals of quartz, plagioclase, and potassium feldspars, but some polycrystalline quartz and subrounded clasts of siltstone are present, suggesting sources from both Paleozoic metasedimentary rocks and volcanic rocks of probable Cenozoic age. Glass shards and tephra were likely deposited as air fall or reworked by rivers and streams into a lacustrine environment.

Zircons separated from the tuffaceous sandstone at the base of the section (ELM11-PN19; Figure 2) and dated by U-Pb LA-ICP-MS returned an Oligocene maximum depositional age of 24.4 ± 0.8 Ma. This is significantly younger than the ~31.1 Ma tuff of Hackwood Ranch and the underlying Eocene volcanic rocks of the Robinson Mountain volcanic field, and provides direct evidence that this exposure (and those stratigraphically above it) is of the Humboldt Formation, rather than representing sediments of the "Indian Well Formation," as previously mapped (Smith and Ketner, 1978). This age of ~24 Ma is significantly older than previous estimates of ~15.4 Ma for the beginning of deposition in Huntington Valley (Perkins et al., 1998; Wallace et al., 2008), but it represents a maximum depositional age, so deposition could have occurred later.

Clasts resembling local Paleozoic sedimentary rocks and Eocene volcanic rocks are more prevalent in conglomeratic sandstones at other locations near the base of the Humboldt Formation (e.g. 40.508581°W, 115.881708°W, WGS84, sample 12HBD03; 40.505784°N, 115.870215°W, WGS84, sample TIWS-J4; Figure 2). At these locations, rounded to subangular clasts (up to 6 cm) of local Eocene volcanic rocks (especially subvolcanic intrusions and the tuff of Dixie Creek), as well as tan siltstone and orange, red, purple, brown, and tan chert and quartzite, are likely derived from local Paleozoic rocks. Conglomerate horizons are typically interbedded with sandstone and siltstone. In thin section (sample 12HBD03), the matrix is composed of clay and silt, with low proportions of carbonate (Figures 21B–C). Few to no loose glass shards are observed in this basal sample (but it does contain rounded clasts of welded ignimbrite, which themselves contain glass shards); it is composed instead mostly of subrounded to subangular clasts of felsic, biotite-rich volcanic rocks, minor amounts of microcrystalline volcanic rocks that appear to be of intermediate to mafic composition, siltstone, and fragments of quartz, plagioclase, biotite, and sanidine (Figures 21B–C). This sample contains clusters of complexly zoned plagioclase that are characteristic of the tuff of Dixie Creek and related subvolcanic intrusions and rhyolite lavas. Thus, these lower exposures of the Humboldt Formation contain significant amounts of detrital material that resemble rocks eroded from the nearby exposed Eocene Robinson Mountain volcanic field.

The proportion of glass shards increases stratigraphically above these exposures. For example, a moderate proportion (15%) of glass shards is observed in thin section in the stratigraphically higher sandstone sample TIWS-J4 (Figure 21D). This sample contains similar mineralogy, but also minor clinopyroxene crystals (<1% of total). A Miocene maximum depositional age of 15.6 ± 0.1 Ma was determined

for the sandstone matrix at this location (sample TIWS-J4). This age is very similar to the oldest Humboldt Formation deposits in Huntington Valley reported previously (Perkins et al., 1998; Wallace et al., 2008). This particular locality and that of the underlying sample 12HBD03 (Figure 2) were also previously included in the (now abandoned) "Indian Well Formation" map unit by Smith and Ketner (1978).

In general, the western exposures of the Humboldt Formation, to the west of Cedar Ridge and Red Spring (Figure 1B), become finer and more carbonate-rich upward (Figure 2). Above the lowest exposures of conglomeratic sandstone, the Humboldt Formation transitions to sandstone, siltstone, and marl, with interbedded limestone and calcic conglomerate beds (Smith and Ketner, 1976). Poorly consolidated, white, light tan, and light blue-grey horizons of mostly volcanic ash are interbedded with the Humboldt Formation above the basal conglomeratic sandstones (Figure 2). Ash (Figure 2) was deposited as air fall, likely from large silicic eruptions in the Snake River Plain (Perkins et al., 1998; Perkins and Nash, 2002; Wallace et al., 2008), but may have been reworked by fluvial action in places. Ash beds range from ~5–20 m thick and produce distinctive sparkly, grey-white soil where exposed.

In thin sections of the stratigraphically lower vitric tuff horizons (samples ELM11-PN13 and TIWS-J3), glass shards are much more prevalent than other clasts. ELM11-PN13, which is a sample of the lowest light-colored vitric tuff horizon exposed, is immediately above the basal sandstones and conglomerates and is composed almost exclusively of strongly aligned glass shards (~97%), with rare crystals of plagioclase, sanidine, opaque oxides, accessory zircon and apatite(?), and essentially no calcite (Figure 21E–F). In thin section of an overlying tuff horizon (TIWS-J3; Figure 21G), calcite composition is much greater (~60%), reflecting increasing amounts of carbonate upward.

Similar maximum depositional ages, within error, of 15.78 ± 0.45 Ma and 15.51 ± 0.44 Ma, were determined using $^{40}Ar/^{39}Ar$ geochronology of sanidine for ELM11-PN13 and ELM11-PN11, respectively. These samples were collected on the lowermost vitric air fall tuff horizon, ~5.6 km apart and roughly along strike of one another. Their age is also the same within error as that of the underlying uppermost conglomeratic sandstone (TIWS-J4, above). A younger $^{40}Ar/^{39}Ar$ sanidine age of 14.62 ± 0.41 Ma was obtained for the stratigraphically higher vitric tuff sample TIWS-J3 described above. A $^{40}Ar/^{39}Ar$ sanidine age of 12.35 ± 0.35 Ma was obtained for the uppermost vitric tuff (sample ELM11-PN2) exposed west Red Spring and Cedar Ridge (Figures 1 and 2).

East and northeast of Cedar Ridge (Figure 1B), the Humboldt Formation is partially duplicated by normal faults that expose Paleozoic strata (Wallace et al., 2008). The lowest stratigraphic levels east of the fault overlie what appears to be the Elko Formation (though these deposits remain undated) and include conglomeratic sandstone having clasts derived from nearby Paleozoic metasiltstones, shales, limestones, and silty limestones. In thin section, sample 12HBD06 (Figure 21H) is a poorly sorted, clast-supported pebbly sandstone composed mostly of coarse sand and small pebbles in a matrix of clay and silt. White mica that might suggest RMEH sediment provenance is minimal to nonexistent in both matrix and clasts. U-Pb analysis by LA-ICP-MS was conducted on this sample but maximum depositional age is uncertain due to the analysis of only one Miocene (15.7 ± 0.5 Ma) grain. A weighted mean age of 38.7 ± 1.7 Ma was determined for 3 Eocene grains in this sample. Because this sample was collected near the contact with the underlying Elko Formation, and because it includes clasts of Paleozoic rocks, the detrital zircon age signal in this sample is thought to be overwhelmed by local pre-Miocene grains. For this reason, the Miocene grain is thought to approximate the maximum depositional age better than the Eocene age.

Dark blue-grey chert is exposed in places north and northeast of Cedar Ridge (Figure 1B), where it occurs in some places as thin (cm-scale) horizons parallel to bedding in volcanic ash horizons, and elsewhere as large areas (>0.3 $km^2$) of faintly bedded chert whose margins do not appear to be controlled strictly by bedding orientation. The latter areas occur near fault zones that expose lower Cenozoic and Paleozoic strata, and are likely formed by silica precipitation from hydrothermal fluids (Figure 21I). Close proximity to mapped normal faults near Cedar Ridge, as well as extremely high $^{204}Pb$ (common Pb) concentrations in high-U detrital zircons of a wide range of ages (>1000 CPS $^{204}Pb$, measured by LA-ICP-MS) from a sample collected near a large area of chert to the northeast of Cedar Ridge (12HBD06) provide further evidence of hydrothermal alteration in that area.

The uppermost strata of the Humboldt Formation in the map area (Figure 2), northeast of Cedar Ridge (Figure 1B), are light tan to light gray, poorly consolidated marls, siltstones, sandstones, and pebbly sandstones with interbedded vitric tuffs. These uppermost strata (Figure 2) contain clasts likely derived from the RMEH (samples 12HBD05 and 12HBD09). Clasts of strained quartzite, some of which contain muscovite or epidote, are observed in thin section in sandstones (sample 12HBD05; Figure 21J–K) and pebble conglomerates at the eastern edge of the map area (e.g. 40.573984°N, 115.731693°W, WGS84). These clasts, which occur together with clasts of metasiltstone, arkosic quartzite, chert, and shale, strongly suggest input from metamorphic rocks of the RMEH. In addition, minor detrital zircon populations between 55–90 Ma and more significant peaks in the Precambrian (Lund Snee, 2013) support RMEH provenance. Monocrystalline grains of quartz, microcline, plagioclase, muscovite, and calcite are observed in thin section. Minor amounts (~2%) of volcanic glass shards are also visible in this sample. A U-Pb LA-ICP-MS maximum depositional age of 14.2 ± 0.2 Ma was determined for this sample from the

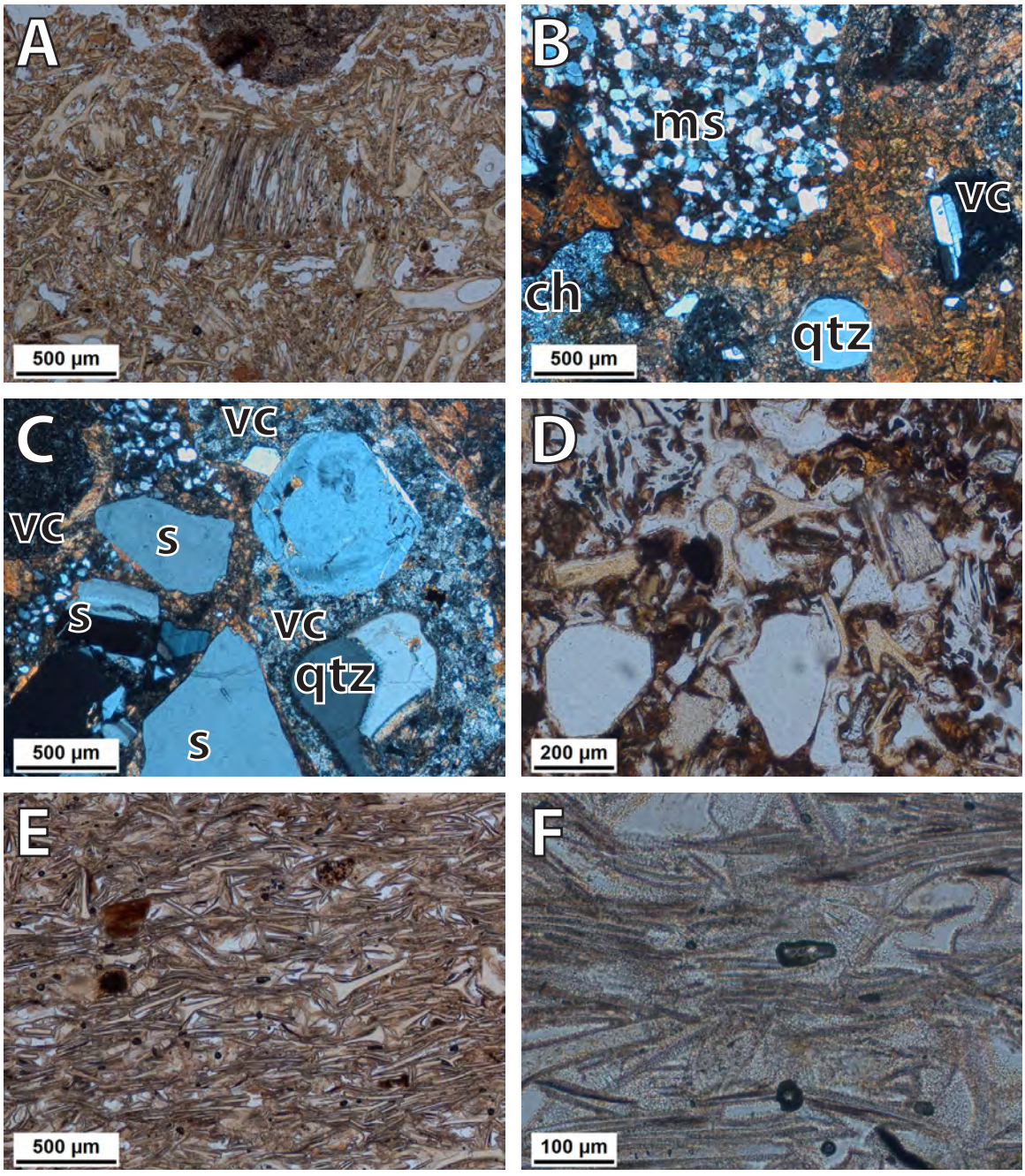
A
500 µm
B
ms
vc
ch
qtz
500 µm
C
vc
vc
s
s
vc
qtz
s
500 µm
D
200 µm
E
500 µm
F
100 µm

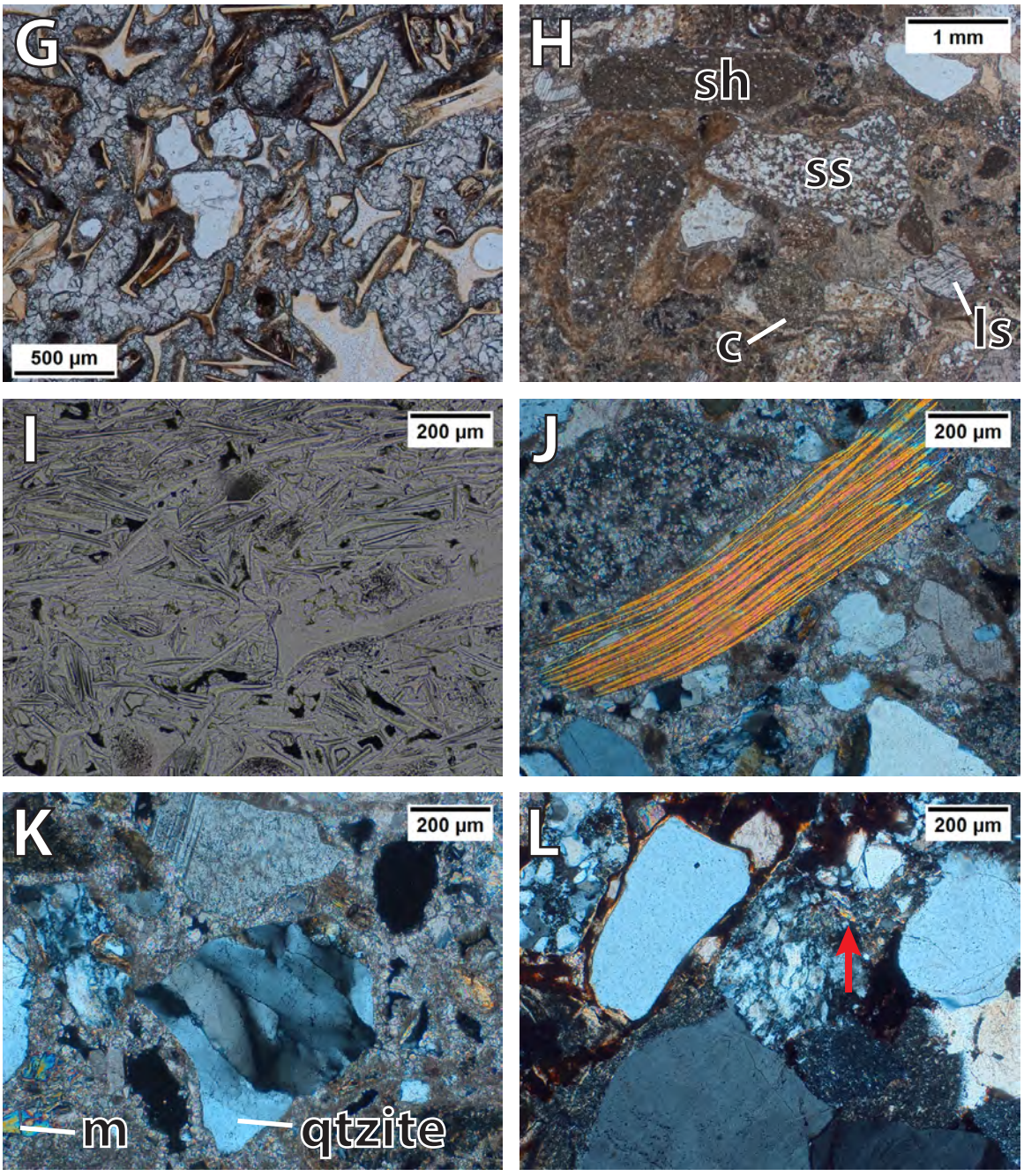
G
500 µm
H
1 mm
sh
ss
c
ls
I
200 µm
J
200 µm
K
200 µm
m
qtzite
L
200 µm

Figure 21: Photomicrographs of the Humboldt Formation and associated rocks. (A) Ash-rich sample at the base of the Humboldt Formation (sample ELM11-PN19), PPL. (B) Pebble conglomerate at a different exposure near the base of the Humboldt Formation (sample 12HBD03), XPL. The matrix is mostly mud and silt, with scarce carbonate. Lithics of metasiltstone (ms), chert (ch), porphyritic volcanics (vc), and quartz are visible. (C) An additional view of silt- and sand-sized clasts of quartz, sanidine (s), and volcanic clasts in basal Humboldt Formation pebbly sandstone (sample 12HBD03), XPL. (D) Clast-supported sandstone (sample TIWS-J4) from an exposure of pebbly sandstone and pebble conglomerate near the base of the Humboldt Formation but stratigraphically above samples ELM11-PN19 and 12HBD03, and immediately below the lowest vitric tuff layer, PPL. (E) The lowest Miocene vitric tuff in the Humboldt Formation exposed in the map area (sample ELM11-PN13), PPL. The matrix is almost exclusively ash shards, with minor crystals. (F) Accessory zircon and apatite(?) surrounded by glass shards in the lowest Miocene vitric tuff (sample ELM11-PN13), PPL. (G) Sparry calcite in the matrix of a Miocene vitric tuff in the Humboldt Formation (sample TIWS-J3; Figure 2), PPL. (H) Pebbly sandstone at the lowest stratigraphic level of the Humboldt Formation northeast of Cedar Ridge (sample 12HBD06), PPL. Subrounded to rounded clasts of limestone (ls), siltstone (ss), and shale (sh) lithics, as well as subangular–angular crystals and ovoid concretions (c). (I) Silicified volcanic glass shards and opaque oxides make up dense, vaguely bedded chert (sample 12JLS227), PPL. (J) A large muscovite crystal (bright interference colors), along with clasts of limey shale, quartzite, limestone, and monocrystalline quartz, calcite, and feldspars (sample 12HBD05), XPL. Muscovite and strained quartzite suggest a sediment source from metamorphic rocks in the RMEH. (K) Clasts of quartzite (qtzite) with strain textures in a limestone matrix (sample 12HBD05), XPL. Detrital muscovite (m) and calcite are also present in this pebbly sandstone near the stratigraphically highest Humboldt Formation deposits exposed in the map area (Figure 2). (L) Clast-supported pebbly sandstone of the Humboldt Formation with the youngest maximum depositional age obtained in this study, indicating the uppermost stratigraphic level of the Humboldt Formation dated (sample 12HBD09), XPL. Muscovite is minor and is observed in quartzite clasts (indicated by the arrow). Other clasts are shale and monocrystalline quartz and calcite. The matrix is mostly muds and silt.

weighted mean of 9 zircon grains.

Other samples at upper stratigraphic levels do not contain abundant muscovite. In thin section, a poorly sorted, poorly cemented pebbly sandstone (12HBD09) contains lithics composed of porphyritic volcanic rocks, metasiltstone, limestone, chert, and deformed quartzite (Figure 21L). Only very minor amounts (<<1%) of white mica are observed, and these are typically found within metasedimentary clasts. Despite the lack of abundant white mica, the occurrence of strained quartzites and large monocrystalline potassium feldspar suggest input from the RMEH. This sample (12HBD09) contains few shards of volcanic glass and has a U-Pb LA-ICP-MS maximum depositional age of 8.2 ± 0.2 Ma. This is the youngest maximum depositional age for the Humboldt Formation measured in the region (Wallace et al., 2008; Colgan et al., 2010). The youngest age previously obtained in Huntington Valley (east of Huntington Creek) was 9.9 Ma (Wallace et al., 2008), and the youngest age obtained by Colgan et al. (2010) west of the Harrison Pass Pluton (in Toyn Creek) using $^{40}Ar/^{39}Ar$ (sanidine) was 11.6 ± 0.05 Ma.

## Associated andesite volcanic rocks (Ta)

Platy, columnar jointed, dark grey andesite (by whole rock geochemistry; "Ta") is exposed in the northeastern part of the study area (Figure 22B) in ~3 dome-shaped structures (e.g. 40.598131°N, 115.746121°W, WGS84). These rocks may represent flow deposits or near-surface dikes or sills. These rocks may intrude adjacent Eocene sedimentary rocks including what appears to be the Elko Formation, suggesting that they may be Eocene or younger in age. These rocks are not in direct map contact with the Miocene Humboldt Formation, so their timing cannot be constrained more precisely at present. Smith and Howard (1977) labeled this unit "Andesite and basaltic andesite and basalt" (Tb) of Upper Miocene age, but Smith and Ketner (1978) apply the Tb label to "andesite and basaltic andesite" elsewhere in the map area (here designated Tba).

In thin section (sample 12JLS225), phenocrysts (~20%) are small (≤1 mm) and reside in a trachytic groundmass of plagioclase laths (≤200 μm long), clinopyroxene, opaque oxides, and glass. Phenocrysts include clinopyroxene, plagioclase, and small amounts of a green mineral that is probably altered hornblende (Figures 22B–C). Most phenocrysts have minor reactions rims and some have shallow embayments (Figures 22B–C), indicating minor to moderate melt disequilibrium.

## Pliocene–Pleistocene Hay Ranch Formation (QThr)

The Hay Ranch Formation (Regnier, 1960; Smith and Ketner, 1976) consists of very shallowly dipping tan, poorly consolidated conglomerate, sandstone, and siltstone. It is best exposed on the western flanks of Cedar Ridge (e.g. 40.441936°N, 115.841840°W, WGS84; Figure 1B), where it records deposition of angular and subangular clasts of siltstone, grey limestone, and quartzite eroded from Paleozoic rocks exposed on Cedar Ridge (Smith and Ketner, 1976, 1978). The poorly sorted deposits are composed of clast-

supported conglomerate lenses interlayered with sandstone and siltstone.

Fossils and zircon fission-track dating indicate a maximum depositional age of middle Pliocene to middle Pleistocene (Smith and Ketner, 1976). It likely that the Hay Ranch Formation was deposited during slip on the west-dipping fault along the west side of Cedar Ridge, because slip on this fault system occurred in part after deposition of the Miocene Humboldt Formation (Wallace et al., 2008; Lund Snee, 2013). Nevertheless, the shallow dips of this unit in the mapped area indicate that any syn- or post-depositional fault slip was minor.

## Quaternary older gravels (Qog) and alluvium (Qal)

Quaternary gravel deposits often cap hillsides and are cut by streams whose bottoms are filled with younger Quaternary sediments. The gravels are extremely poorly sorted, consisting of pebbles, cobbles, and boulders ~1 cm–10 m in diameter. Where clearly exposed, only boulders are visible, but associated sand and silt have likely been washed away by younger fluvial action. Clasts predominantly include recognizable Paleozoic and Cenozoic lithologies, especially Diamond Peak Formation conglomerates and Cenozoic subvolcanic intrusive rocks, ignimbrites, dacite lavas, and dark grey basalts or basaltic andesites. The deposits appear crudely bedded in aerial photographs and form broad, flat slopes that likely covered a Quaternary pediment surface that is presently being incised. In other places, particularly on steep slopes, the gravels are overlain by a veneer of younger alluvium.

## SUMMARY AND REGIONAL IMPLICATIONS

Huntington Valley is situated east of the Piñon Range, in the hanging wall of a shallowly west-dipping detachment system bounding the west side of the Ruby Mountains–East Humboldt Range (RMEH) metamorphic core complex. This geologic map of Cenozoic sedimentary, volcanic, and subvolcanic rocks of the central Robinson Mountain volcanic field and northwestern Huntington Valley provides important information about the history of Cenozoic crustal extension, magmatism, sedimentation, and paleogeography near the RMEH.

Depositional rates in the Elko Basin were minor from Cretaceous to Oligocene time, and became rapid in the Middle Miocene. Late Cretaceous(?)–Eocene(?) conglomerate, sandstone, siltstone, and limestone "redbeds" (TKcs) and limestone (TKl) are exposed at the base of the Cenozoic section in places, where they each reach thicknesses of ~600 m, but they are not exposed at all in other locations. The overlying Eocene Elko Formation is only ~180 m thick at its greatest in the map area. Detrital zircon geochronology conducted on two samples collected near its base yields a maximum depositional age of ~45.9 ± 1.0 Ma, and a third sample collected near the top of this unit yields a maximum depositional age of 37.9 ± 0.5 Ma.

The calcic to calc-alkalic Robinson Mountain volcanic field records early peraluminous to weakly metaluminous "ignimbrite flare-up" volcanism of basaltic andesite to trachydacite and rhyolite composition, which occurred mostly between about 38.5–36.8 Ma. Early eruptions were roughly synchronous with the end of deposition of the Elko Formation, and no significant unconformity is observed beneath the volcanic units. The only Eocene–Oligocene sedimentary rocks exposed above the Eocene Elko Formation are thin, fluviolacustrine deposits interbedded within the volcanic rocks. For this reason, the "Indian Well Formation" name for Eocene–Oligocene volcanic and sedimentary rocks has been abandoned. The rhyolitic, Oligocene-age tuff of Hackwood Ranch is significantly younger than the Eocene deposits of the Robinson Mountain volcanic field. This tuff was erupted at ~31.1 Ma, which coincides with a lull in regional volcanism, but could represent far-traveled deposits from a distant volcanic center.

Significant, approximately westward tilting developed a shallow angular unconformity between ~37.3–33.9 Ma (10–15°). Subsequently, between ~31.1 Ma and 24.4 Ma or later (10–15°additional westward tilting occurred. These westward tilting events were likely associated with slip on east-dipping normal faults in the Piñon Range. Following the second episode of westward tilting, a basin rapidly developed near the present-day RMEH, as recorded by thick deposits of the mostly Miocene Humboldt Formation that dip gently eastward toward the RMEH. Greater than 1 km of the sedimentary strata previously mapped as Eocene–Oligocene age has been reassigned to the Miocene Humboldt Formation as a result of our geologic mapping and supporting geochronology.

Detrital zircon geochronology yielded a coherent age group at ~24.4 Ma for one tuffaceous pebble conglomerate and sandstone sample at the base of the Humboldt Formation, but it is unlikely that this maximum depositional age constrains the timing of the start of basin sedimentation. Deposition accelerated at ~16–15 Ma, when most of Humboldt Formation pebble conglomerate, sandstone, siltstone, marl, and air-fall tuff were deposited in Huntington Valley. Locally, pre-Tertiary rocks were exposed by faulting by ~16 Ma (although this depositional age is not well constrained), and RMEH provenance is not detected until ~14 Ma, suggesting that the metamorphic core complex was not exposed until about this time. Greater than 2100 m of Humboldt Formation strata were deposited in the study area alone (thickening further eastward toward the RMEH), and deposition continued until at least ~8.2 Ma, but the rate apparently decreased before ~12 Ma.

Miocene or later fault slip occurred along a well-preserved, east-dipping normal fault system exposed at the

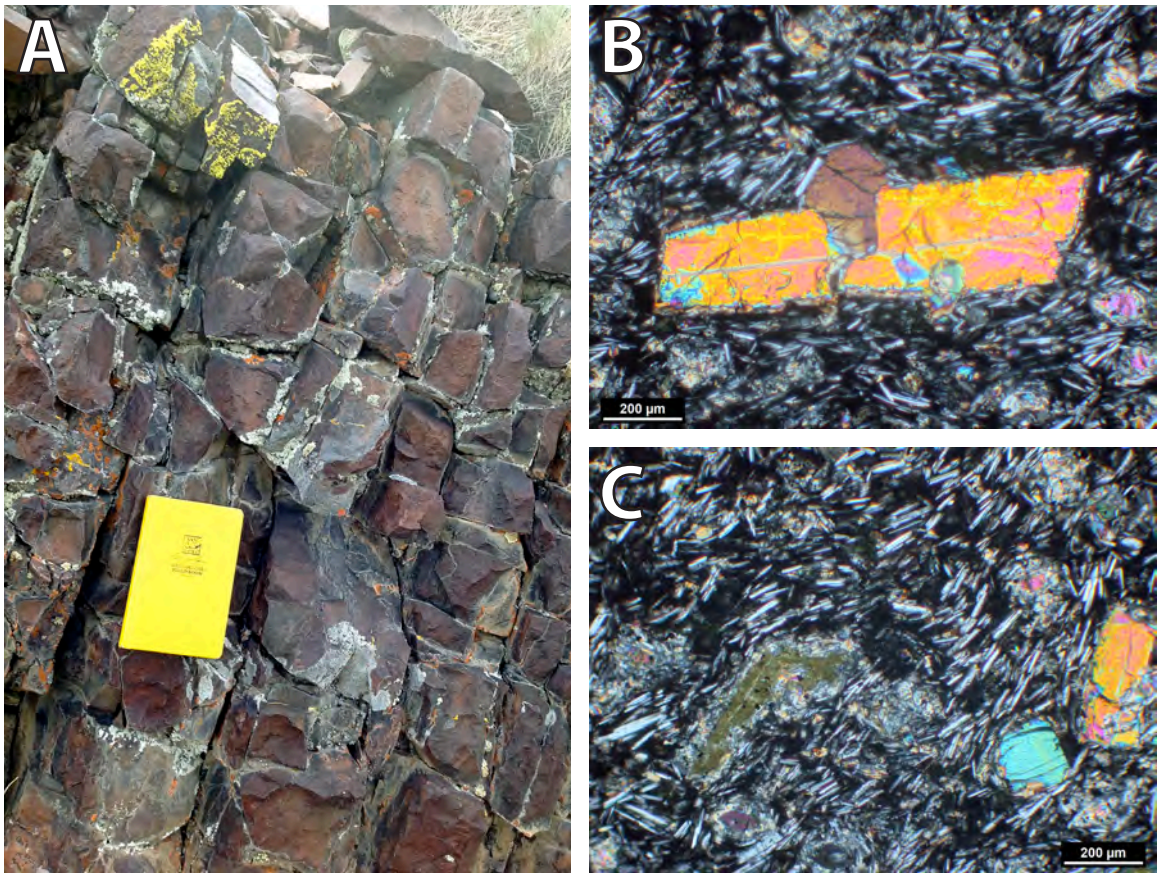


Figure 22: (A) Photograph of basaltic andesite from a cinder cone at the northeast corner of the map area. (B) Photomicrograph showing clinopyroxene phenocryst in trachytic groundmass of the basaltic andesite (sample 12JLS225), XPL. (C) Photomicrograph showing phenocrysts of clinopyroxene (east edge) and apparently altered green hornblende (west-center) in a trachytic groundmass of the basaltic andesite (sample 12JLS225), XPL.

east side of the Piñon Range, partially synchronous with faulting at the RMEH. Uplift and erosion of Eocene- to Quaternary-age sedimentary and volcanic deposits on the west side of Huntington Valley support a significant magnitude of slip on west-dipping normal faults west of the study area during or after Miocene time. Open folding of the Humboldt Formation occurred during or after the Middle–Late Miocene, perhaps due to normal fault slip offsetting underlying Paleozoic basement.

This geologic mapping study thus supports the hypothesis that surface-breaking extensional faulting in and near the mapped area was minor from the Late Cretaceous(?) through the Early Miocene, and that most surface-breaking extension and sediment deposition occurred in Middle Miocene time.

## ACKNOWLEDGEMENTS

Mapping was funded by Stanford University and U.S. Geological Survey EdMap award number G12AC20189 to Lund Snee and Miller and NSF grant Tectonics 1322084 to Miller. We thank Joe Colgan, Dave John, and Chris Henry for contributing their extensive knowledge about the region (and unpublished data) and helping launch this project. We also thank Hunter Dudley, Monica Erviti, Jeff Knox, Mark Raftrey, and the students of GES 190 for their able assistance in the field. Beti Girma and Samuel Xiao helped digitize the map. We are grateful for NBMG editorial and cartographic assistance by Kathryn E. Ryan.

## REFERENCES

Best, M. G., Barr, D. L., Christiansen, E. H., Gromme, S., Deino, A. L., and Tingey, D. G. 2009. The Great Basin Altiplano during the middle Cenozoic ignimbrite flareup: insights from volcanic rocks. *International Geology Review*, 51(7-8):589–633.

Chamberlain, C. P., Mix, H. T., Mulch, A., Hren, M. T., Kent-Corson, M. L., Davis, S. J., Horton, T. W., and Graham, S. A. 2012. The Cenozoic climatic and topographic evolution of the western North American Cordillera. *American Journal of Science*, 312:213–262.

Chetel, L. M., Janecke, S. U., Carroll, A. R., Beard, B. L., Johnson, C. M., and Singer, B. S. 2011. Paleogeographic reconstruction of the Eocene Idaho River, North American Cordillera. *GSA Bulletin*, 123(1/2):71–88.

Cline, J. S., Hofstra, A. H., Muntean, J. L., Tosdal, R. M., and Hickey, K. A. 2005. Carlin-type gold deposits in Nevada: Critical geologic characteristics and viable models. *Economic Geology*, 100th anniversary volume:451–484.

Coats, R. R. 1987. Geology of Elko County, Nevada. *Nevada Bureau of Mines and Geology Bulletin 101*, pages 1–112.

Colgan, J. P. and Henry, C. D. 2009. Rapid middle Miocene collapse of the Mesozoic orogenic plateau in northcentral Nevada. *International Geology Review*, 51(9):920–961.

Colgan, J. P., Howard, K. A., Fleck, R. J., and Wooden, J. L. 2010. Rapid middle Miocene extension and unroofing of the southern Ruby Mountains, Nevada. *Tectonics*, 29(TC6022):38 p.

DeCelles, P. G. 2004. Late Jurassic to Eocene evolution of the Cordilleran thurst belt and foreland basin system, western U.S.A. *American Journal of Science*, 304:105–168.

Dickinson, W. R. 2006. Geotectonic evolution of the Great Basin. *Geosphere*, 2(7):358–368.

Druschke, P., Hanson, A. D., Wells, M. L., Gehrels, G. E., and Stockli, D. 2011. Paleogeographic isolation of the Cretaceous to Eocene Sevier hinterland, east-central Nevada: Insights from U-Pb and (U-Th)/He detrital zircon ages of hinterland strata. *GSA Bulletin*, 123(5–6):1141–1160.

Druschke, P., Hanson, A. D., Wells, M. L., Rasbury, T., Stockli, D. F., and Gehrels, G. 2009. Synconvergent surface-breaking normal faults of Late Cretaceous age within the Sevier hinterland, east-central Nevada. *Geology*, 37(5):447–450.

Faulds, J. E., Henry, C. D., and Hinz, N. H. 2005. Kinematics of the northern Walker Lane: An incipient transform fault along the Pacific–North American plate boundary. *Geology*, 33(6):505–508.

Fouch, T. D., Hanley, J. H., and Forester, R. M. 1979. Preliminary correlation of Cretaceous and Paleogene lacustrine and related nonmarine sedimentary and volcanic rocks in parts of the eastern Great Basin of Nevada and Utah. In *Basin and Range Symposium*, pages 305–312. Rocky Mountain Association of Geologists.

Gordee, S. M., Dettloff, C. L., and Burton, B. R. 2000. Geologic and geochemical comparison of Late Eocene–Oligocene volcanic and intrusive rocks, Carlin-Piñon Range and central Ruby Mountains, Elko County, Nevada. *Geological Society of America Abstracts with Programs*, 32(7):159.

Hague, A. and Emmons, S. F. 1877. Descriptive geology: Geological exploration of the Fortieth Parallel, Vol. II. *Professional Papers of the Engineering Dept, US Army*, 18.

Haxby, W. F., Melkonian, A. K., Coplan, J., Chan, S. M., and Ryan, W. B. F. 2010. GeoMapApp freeware software, v. 2.3. *Lamont-Doherty Earth Observatory, Palisades, http://jgs. geoscienceworld. org/cgi/content/-full/168/2/333*.

Haynes, S. R. 2003. Development of the Eocene Elko basin, northeastern Nevada: Implications for paleogeography and regional tectonism. Master's thesis, The University of British Columbia.

Henrici, A. C. and Haynes, S. R. 2006. Elkobatrachus brocki, a new pelobatid (Amphibia: anura) from the Eocene Elko Formation of Nevada. *Annals of Carnegie Museum*, 75(1):11–35.

Henry, C. D., Hinz, N. H., Faulds, J. E., Colgan, J. P., John, D. A., Brooks, E. R., Cassel, E. J., Garside, L. J., Davis, D. A., and Castor, S. B. 2012. Eocene–Early Miocene paleotopography of the Sierra Nevada–Great Basin–Nevadaplano based on widespread ash-flow tuffs and paleovalleys. *Geosphere*, 8(1):1–27.

Henry, C. D. and John, D. A. 2013. Magmatism, ash-flow tuffs, and calderas of the ignimbrite flareup in the western Nevada volcanic field, Great Basin, USA. *Geosphere*, 9(4):951–1008.

Horton, T. W. and Chamberlain, C. P. 2006. Stable isotopic evidence for Neogene surface downdrop in the central Basin and Range Province. *GSA Bulletin*, 118(3/4):475–490.

Horton, T. W., Sjostrom, D. J., Abruzzese, M. J., Poage, M. A., Waldbauer, J. R., Hren, M., Wooden, J., and Chamberlain, C. P. 2004. Spatial and temporal variation of cenozoic surface elevation in the Great Basin and Sierra Nevada. *American Journal of Science*, 304:862–888.

John, D. A., Henry, C. D., and Colgan, J. P. 2008. Magmatic and tectonic evolution of the Caetano caldera, north-central Nevada: A tilted, mid-Tertiary eruptive center and source of the Caetano Tuff. *Geosphere*, 4(1):75–106.

Ketner, K. B. 1990. Geologic Map of the Elko Hills, Elko County, Nevada. *Geological Survey Miscellaneous Investigations I-2082*.

Ketner, K. B. 1998. The nature and timing of tectonism in the western facies terrane of Nevada and California: An outline of evidence and interpretations derived from geologic maps of key areas. *U.S. Geological Survey Professional Paper 1592*, pages 1–19.

Ketner, K. B. and Alpha, A. G. 1992. Mesozoic and Tertiary rocks near Elko, Nevada—Evidence for Jurassic to Eocene folding and low-angle faulting. *Evolution of sedimentary basins—Eastern Great Basin: US Geological Survey Bulletin 1988-C*, pages C1–C13.

Ketner, K. B. and Smith, J. F. 1963. Geology of the Railroad mining district, Elko County, Nevada. *U.S. Geological Survey Professional Paper 1162–B*, pages B1–B27.

King, C. 1878. Systematic geology: Geological Exploration of the Fortieth Parallel, Vol. I. *Professional Papers of the Engineering Dept, US Army*, 18.

Le Bas, M. J., Le Maitre, R. W., Streckeisen, A., and Zanettin, B. 1986. A chemical classification of volcanic rocks based on the total alkali-silica diagram. *Journal of petrology*, 27(3):745–750.

Lund Snee, J.-E. 2013. Geology and geochronology of Cenozoic units in the Piñon Range and Huntington Valley, Nevada. Master's thesis, Stanford University, Stanford, CA.

Lund Snee, J.-E., Miller, E. L., Grove, M., and Hourigan, J. K. Cenozoic paleogeographic evolution of the Elko Basin and surrounding region, northeast Nevada. *Geosphere (submitted)*.

Moore, S. W., Madrid, H. B., and Server, G. T. 1983. Results of oil-shale investigations in northeastern Nevada. *U.S. Geological Survey Open File Report 83-586*, pages C1–C18.

Palmer, H. C., MacDonald, W. D., and Hayatsu, A. 1991. Magnetic, structural and geochronologic evidence bearing on volcanic sources and Oligocene deformation of ash flow tuffs, northeast Nevada. *Journal of Geophysical Research*, 96(B2):2185–2202.

Perkins, M. E., Brown, F. H., Nash, W. P., Williams, S. K., and McIntosh, W. 1998. Sequence, age, and source of silicic fallout tuffs in middle to late Miocene basins of the northern Basin and Range province. *Geological Society of America Bulletin*, 110(3):344–360.

Perkins, M. E. and Nash, B. P. 2002. Explosive silicic volcanism of the Yellowstone hotspot: The ash fall tuff record. *Geological Society of America Bulletin*, 114(3):367–381.

Regnier, J. 1960. Cenozoic geology in the vicinity of Carlin, Nevada. *Geological Society of America Bulletin*, 71(8):1189–1210.

Ressel, M. W. and Henry, C. D. 2006. Igneous geology of the Carlin Trend, Nevada: Development of the Eocene Plutonic Complex and significance for Carlin-type gold deposits. *Economic Geology*, 101:347–383.

Rickwood, P. C. 1989. Boundary lines within petrologic diagrams which use oxides of major and minor elements. *Lithos*, 22(4):247–263.

Ryan, W. B. F., Carbotte, S. M., Coplan, J. O., O'Hara, S., Melkonian, A., Arko, R., Weissel, R. A., Ferrini, V., Goodwillie, A., Nitsche, F., Bonczkowski, J., and Zemsky, R. 2009. Global Multi-Resolution Topography synthesis. *Geochemistry, Geophysics, Geosystems*, 10(3):1–9.

Ryskamp, E. B., Abbott, J. T., Christiansen, E. H., Keith, J. D., Vervoort, J. D., and Tingey, D. G. 2008. Age and petrogenesis of volcanic and intrusive rocks in the Sulphur Spring Range, central Nevada: Comparisons with ore-associated Eocene magma systems in the Great Basin. *Geosphere*, 4(3):496–519.

Satarugsa, P. and Johnson, R. A. 2000. Cenozoic tectonic evolution of the Ruby Mountains metamorphic core complex and adjacent valleys, northeastern Nevada. *Rocky Mountain Geology*, 35(2):205–230.

Server, G. T. and Solomon, B. J. 1983. Geology and oil shale deposits of the Elko Formation, Pinon Range, Elko County, Nevada. *Geological Survey Miscellaneous Field Studies Map MF-1546*.

Sharp, R. P. 1939. The Miocene Humboldt Formation in northeastern Nevada. *The Journal of Geology*, 47(2):133–160.

Smith, J. F. and Howard, K. A. 1977. Geologic map of the Lee Quadrangle (1:62,500 scale). *US Geological Survey Map GQ-1393*.

Smith, J. F. and Ketner, K. B. 1975. Stratigraphy of Paleozoic rocks in the Carlin-Piñon Range area, Nevada. *U.S. Geological Survey Professional Paper 867–A*, pages A1–A87.

Smith, J. F. and Ketner, K. B. 1976. Stratigraphy of post-Paleozoic rocks and summary of resources in the Carlin-Piñon Range area, Nevada. *U.S. Geological Survey Professional Paper 867–B*, pages B1–B48.

Smith, J. F. and Ketner, K. B. 1978. Geologic map of the Carlin-Pinon Range area, Elko and Eureka counties, Nevada. *U.S. Geological Survey Miscellaneous Investigations Series I-1028*.

Solomon, B. J., McKee, E. H., and Andersen, D. W. 1979. Stratigraphy and depositional environments of Paleogene rocks near Elko, Nevada. In *Pacific Coast Paleogeography Symposium 3: Cenozoic Paleogeography of the Western United States*, pages 75–88. Pacific Section, SEPM (Society for Sedimentary Geology).

Stewart, J. H. 1980. Geology of Nevada. *Nevada Bureau of Mines and Geology Special Publication 4*, pages 1–136.

Trexler, J. H., Cashman, P. H., Snyder, W. S., and Davydov, V. I. 2004. Late Paleozoic tectonism in Nevada: Timing, kinematics, and tectonic significance. *GSA Bulletin*, 116(5/6):525–538.

Trexler, J. H. and Nitchman, S. P. 1990. Sequence stratigraphy and evolution of the Antler foreland basin, east-central Nevada. *Geology*, 18:422–425.

Walker, J., Geissman, J., Bowring, S., and Babcock, L. 2012. Geologic time scale v. 4.0. *Boulder: Geological Society of America*.

Wallace, A. R., Perkins, M. E., and Fleck, R. J. 2008. Late Cenozoic paleogeographic evolution of northeastern Nevada: Evidence from the sedimentary basins. *Geosphere*, 4(1):36–74.